Frontiers of Information Technology & Electronic Engineering
www.jzus.zju.edu.cn; engineering.cae.cn; www.springerlink.com
ISSN 2095-9184 (print); ISSN 2095-9230 (online)
E-mail: jzus@zju.edu.cn

Beamforming and fronthaul compression design for intelligent reflecting surface aided cloud radio access networks*

Yu ZHANG[†‡1,2], Xuelu WU[1], Hong PENG[†1], Caijun ZHONG[†3], Xiaoming CHEN[†3]

[1]*College of Information Engineering, Zhejiang University of Technology, Hangzhou 310023, China*

[2]*National Mobile Communications Research Laboratory, Southeast University, Nanjing 210096, China*

[3]*College of Information Science and Electronic Engineering, Zhejiang University, Hangzhou 310027, China*

[†]E-mail: yzhang@zjut.edu.cn; ph@zjut.edu.cn; caijunzhong@zju.edu.cn; chen_xiaoming@zju.edu.cn

Received June 29, 2021; Revision accepted Nov. 11, 2021; Crosschecked Dec. 13, 2021

Abstract: Owing to the inherent central information processing and resource management ability, the cloud radio access network (C-RAN) is a promising network structure for an intelligent and simplified sixth-generation (6G) wireless network. Nevertheless, to further enhance the capacity and coverage, more radio remote heads (RRHs) as well as high-fidelity and low-latency fronthaul links are required, which may lead to high implementation cost. To address this issue, we propose to exploit the intelligent reflecting surface (IRS) as an alternative way to enhance the C-RAN, which is a low-cost and energy-efficient option. Specifically, we consider the uplink transmission where multi-antenna users communicate with the baseband unit (BBU) pool through multi-antenna RRHs and multiple IRSs are deployed between the users and RRHs. RRHs can conduct either point-to-point (P2P) compression or Wyner-Ziv coding to compress the received signals, which are then forwarded to the BBU pool through fronthaul links. We investigate the joint design and optimization of user transmit beamformers, IRS passive beamformers, and fronthaul compression noise covariance matrices to maximize the uplink sum rate subject to fronthaul capacity constraints under P2P compression and Wyner-Ziv coding. By exploiting the Arimoto-Blahut algorithm and semi-definite relaxation (SDR), we propose a successive convex approximation approach to solve non-convex problems, and two iterative algorithms corresponding to P2P compression and Wyner-Ziv coding are provided. Numerical results verify the performance gain brought about by deploying IRS in C-RAN and the superiority of the proposed joint design.

Key words: Cloud radio access network (C-RAN); Intelligent reflecting surface (IRS); Transmit beamforming; Fronthaul compression

https://doi.org/10.1631/FITEE.2100307 **CLC number:** TN929.5

1 Introduction

With the development of artificial intelligence (AI), Internet of Things (IoT), mobile Internet, and industrial Internet, to provide diversified wireless network services to the whole society, it is necessary to build a cross-scenario, cross-business, reconfigurable, powerful, extremely intelligent, and extremely simplified wireless network, which

‡ Corresponding author

* Project supported by the Zhejiang Provincial Natural Science Foundation of China (Nos. LY21F010008 and LD21F010001), the National Natural Science Foundation of China (No. 62171412), and the Open Research Fund of National Mobile Communications Research Laboratory, Southeast University, China (No. 2020D10)

ORCID: Yu ZHANG, https://orcid.org/0000-0002-9736-8244

integrates communication, computing, caching, and control (the 4Cs) with AI. With this aim, the concept of "intellicise" wireless network (Zhang P et al., 2022) has been proposed, among which the cloud radio access network (C-RAN) is one of the potential candidate network structures (Peng et al., 2020). In a C-RAN, the baseband processing function of conventional base stations is backward migrated into a baseband unit (BBU) pool, and radio remote heads (RRHs) are deployed close to users. Therefore, joint signal processing and flexible resource management can be inherently achieved in a C-RAN. Nevertheless, high-speed fronthaul links are required to connect RRHs and the BBU pool, which leads to high implementation cost and complexity for dense deployment of RRHs (Pizzinat et al., 2015). Therefore, a more cost-effective way to improve the capacity and coverage of C-RAN is required in the face of increase of access equipment and data traffic.

To tackle this issue, we propose to exploit the recently emerging intelligent reflecting surface (IRS) technology to enhance the C-RAN. An IRS consists of a large number of reflection elements, with which controllable phase shifts can be imposed on the impinging waves (Wu and Zhang, 2020). Aided by this, the IRS can generate the desired reflection beams and create favorable propagation conditions. Since the IRS is basically a passive device and solely requires a low-rate control link, it provides an energy-efficient and cost-effective way to enhance the C-RAN. Recently, a lot of works have studied the IRS-assisted wireless communication systems, e.g., multiple-input multiple-output (MIMO) systems (Wu and Zhang, 2018; Guo et al., 2019), simultaneous wireless information and power transfer (SWIPT) (Pan et al., 2020), two-way communication systems (Zhang Y et al., 2020), non-orthogonal multiple access (NOMA) (Zeng et al., 2021), and multi-cell systems (Hua et al., 2021). For IRS-assisted millimeter-wave (mmWave) communication, Zhu et al. (2020) verified the system performance improvement based on stochastic geometry analysis. A low-complexity channel information acquisition method for IRS-assisted mmWave communication systems was proposed in Cui and Yin (2019).

1.1 Related works

One of the main concerns in C-RAN is the capacity-limited fronthaul link between the BBU pool and RRHs, and there are a lot of works considering fronthaul compression optimization to improve the system performance. Del Coso and Simoens (2009) investigated distributed fronthaul compression based on Wyner-Ziv coding at RRHs and optimized the compression noise covariance matrix in a gradient approach. In Park et al. (2013b), optimization of the per-RRH compression noise covariance matrix was proposed. Zhou YH and Yu (2014) considered both point-to-point (P2P) compression and Wyner-Ziv coding at RRHs, and then they optimized the corresponding quantization noise covariance matrices to maximize the uplink sum rate. For both uplink and downlink transmission, the distributed fronthaul compression techniques were surveyed by Park et al. (2014), and the design frameworks were proposed. In the C-RAN scheme in which users and RRHs are equipped with multiple antennas, the user/RRH beamforming and fronthaul compression can be jointly designed to further improve the system performance. Zhou YH and Yu (2016) jointly optimized the user transmit beamforming and fronthaul compression for a C-RAN uplink using the weight minimum-mean-square-error (WMMSE) approach and the successive convex approximation (SCA) approach, and thereafter proposed a low-complexity design under a high signal-to-quantization-noise ratio (SQNR). For the C-RAN downlink, Park et al. (2013a) considered multivariate compression across RRHs and proposed to jointly optimize RRH beamforming and fronthaul compression, wherein a robust design with respect to imperfect channel state information (CSI) was also considered. For the C-RAN with wireless fronthauling, the beamforming corresponding to the fronthaul link (i.e., RRH beamforming for uplink and BBU pool beamforming for downlink) should also be taken into consideration. The joint design for uplink transmission was considered in Park et al. (2017a) and Najafi et al. (2019), and the design for downlink has been assessed by Park et al. (2016, 2017b).

Up to now, there have been limited works devoted to IRS-assisted C-RAN or cell-free networks. Recently, Huang et al. (2021) proposed a distributed design framework to jointly optimize the transmit beamformer and IRS passive beamformer to maximize the weighted sum rate. An IRS-aided wideband cell-free network was considered by Zhang ZJ and Dai (2021), where a joint design was investigated to

maximize the system capacity. Nevertheless, limited fronthaul capacity and fronthaul compression optimization were not addressed in the above works. For the C-RAN with wired fronthaul, Yu et al. (2020) exploited the IRS to improve the accuracy of over-the-air computation. Similarly, Weinberger et al. (2021) investigated methods to obtain the full benefit from the cooperation of rate splitting and IRS techniques to improve the energy efficiency of C-RAN. In addition, Zhang Y et al. (2021) considered the deployment of a single IRS on the wireless fronthaul in a C-RAN and jointly optimized transmit beamforming, IRS passive beamforming, and fronthaul compression using a WMMSE-SCA approach.

1.2 Contributions

The main contributions of this paper are summarized as follows:

1. We consider IRS-assisted C-RAN uplink transmission, wherein multiple IRSs are deployed between multi-antenna users and RRHs. RRHs conduct P2P compression or Wyner-Ziv coding to compress the received uplink signals. We investigate the joint design of user transmit beamforming, IRS passive beamforming, and fronthaul compression under the two compression schemes, with the goal of maximizing the uplink sum rate. To the best of our knowledge, the above joint design has not been investigated in the literature.

2. The design problem is non-convex, wherein the transmit beamformers, passive beamformers, and fronthaul compression noise covariance matrices are coupled. By exploiting the Arimoto-Blahut algorithm (Blahut, 1972) and semi-definite relaxation (SDR), we propose two iterative algorithms based on SCA for the cases of P2P compression and Wyner-Ziv coding, respectively. Moreover, inspired by the results in the conventional C-RAN (Zhou YH and Yu, 2016), we modify the proposed algorithms for high SQNR regime, to reduce the computational complexity.

Note that the design of IRS passive beamforming is coupled with that of fronthaul compression through the fronthaul constraints. Therefore, the joint design investigated in this paper is not a trivial extension of the aforementioned works in conventional C-RAN. Besides, we consider Wyner-Ziv coding with joint decompression instead of sequential decompression as in previous works (Park et al., 2014; Zhou YH and Yu, 2016; Zhang Y et al., 2021), which is more general and leads to different fronthaul constraints. In particular, we propose a novel approach based on the Arimoto-Blahut algorithm to treat the non-convex problem.

Notations used throughout the paper are as follows: For a matrix $\boldsymbol{A}$, $|\boldsymbol{A}|$, $\mathrm{tr}(\boldsymbol{A})$, $\boldsymbol{A}^{\mathrm{T}}$, and $\boldsymbol{A}^{\mathrm{H}}$ denote the determinant, trace, transpose, and conjugate transpose of $\boldsymbol{A}$, respectively. Symbol $\mathrm{diag}(\boldsymbol{A})$ denotes a column vector formed with the diagonals of $\boldsymbol{A}$. For an index set $\mathcal{S}$, unless otherwise specified, $\boldsymbol{A}_{\mathcal{S}}$ denotes the matrix with elements A_i whose indices $i \in \mathcal{S}$ and $\mathrm{diag}\left(\{A_i\}_{i\in\mathcal{S}}\right)$ denotes the block diagonal matrix formed with A_i on the diagonal where $i \in \mathcal{S}$. $\boldsymbol{A} \odot \boldsymbol{B}$ denotes the Hadamard product of $\boldsymbol{A}$ and $\boldsymbol{B}$. $\boldsymbol{I}$ denotes the identity matrix. $\mathbb{E}[\cdot]$ stands for the expectation. Let $\mathcal{K} = \{1, 2, \ldots, K\}$, $\mathcal{L} = \{1, 2, \ldots, L\}$, and $\mathcal{M} = \{1, 2, \ldots, M\}$.

2 System model

We consider the uplink transmission of a C-RAN, where K multi-antenna users communicate with the BBU pool through L RRHs, as depicted in Fig. 1. Each user and each RRH are equipped with N_{U} and N_{R} antennas, respectively. M IRSs are deployed to aid the communication between the users and RRHs, each of which has N_{I} reflection elements. For simplicity, we assume global CSI at the BBU pool. Note that the CSI acquisition for the IRS link has been widely discussed (Cui and Yin, 2019; Wang et al., 2020).

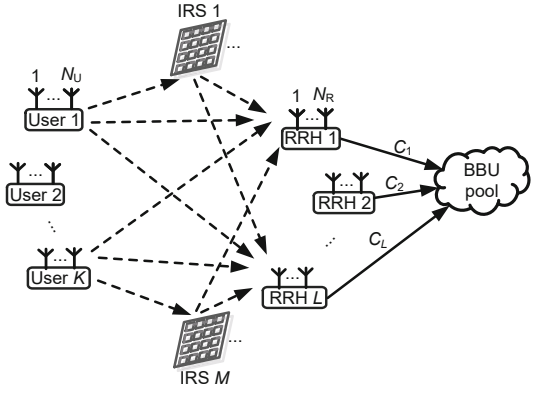

Fig. 1 System model

On the access link, user k ($k \in \mathcal{K}$) transmits the signal to the RRHs, which is given by the following

expression:

$$\boldsymbol{x}_k = \boldsymbol{F}_k \boldsymbol{s}_k, \tag{1}$$

where $\boldsymbol{s}_k \in \mathbb{C}^d$ is the data symbol vector with covariance matrix $\boldsymbol{I}_{N_\mathrm{U}}$ and $\boldsymbol{F}_k \in \mathbb{C}^{N_\mathrm{U}\times d}$ is the user transmit beamformer subject to the power constraint $\mathrm{tr}\left(\boldsymbol{F}_k \boldsymbol{F}_k^{\mathrm{H}}\right) \le P_k$. Then, the signal received by RRH l ($l \in \mathcal{L}$) can be expressed as follows:

$$\begin{aligned}\boldsymbol{y}_l &= \sum_{k=1}^{K} \boldsymbol{H}_{k,l}\boldsymbol{x}_k + \sum_{k=1}^{K}\sum_{m=1}^{M} \boldsymbol{G}_{l,m}\boldsymbol{\Theta}_m \boldsymbol{H}_{k,R,m}\boldsymbol{x}_k + \boldsymbol{n}_l \\ &= \sum_{k=1}^{K} \boldsymbol{H}_{k,l}\boldsymbol{F}_k\boldsymbol{s}_k + \sum_{k=1}^{K} \boldsymbol{G}_{l,\mathcal{M}}\boldsymbol{\Theta}\boldsymbol{H}_{k,R,\mathcal{M}}\boldsymbol{F}_k\boldsymbol{s}_k + \boldsymbol{n}_l \\ &= (\boldsymbol{H}_{\mathcal{K},l} + \boldsymbol{G}_{l,\mathcal{M}}\boldsymbol{\Theta}\boldsymbol{H}_{\mathcal{K},R,\mathcal{M}})\boldsymbol{F}_{\mathcal{K}}\boldsymbol{s}_{\mathcal{K}} + \boldsymbol{n}_l,\end{aligned} \tag{2}$$

where $\boldsymbol{H}_{k,l} \in \mathbb{C}^{N_\mathrm{R}\times N_\mathrm{U}}$, $\boldsymbol{G}_{l,m} \in \mathbb{C}^{N_\mathrm{R}\times N_\mathrm{I}}$, and $\boldsymbol{H}_{k,R,m} \in \mathbb{C}^{N_\mathrm{I}\times N_\mathrm{U}}$ represent the channel matrices between user k and RRH l, between IRS m and RRH l, and between user k and IRS m, respectively. $\boldsymbol{H}_{\mathcal{K},l} = [\boldsymbol{H}_{1,l}, \boldsymbol{H}_{2,l}, ..., \boldsymbol{H}_{K,l}]$ represents the channel matrix between each user and RRH l, $\boldsymbol{G}_{l,\mathcal{M}} = [\boldsymbol{G}_{l,1}, \boldsymbol{G}_{l,2}..., \boldsymbol{G}_{l,M}]$ represents the channel matrix between each IRS and RRH l, $\boldsymbol{H}_{k,R,\mathcal{M}} = [\boldsymbol{H}_{k,R,1}^{\mathrm{T}}, \boldsymbol{H}_{k,R,2}^{\mathrm{T}}, ..., \boldsymbol{H}_{k,R,M}^{\mathrm{T}}]^{\mathrm{T}}$ denotes the channel matrix between user k and each IRS, and $\boldsymbol{H}_{\mathcal{K},R,\mathcal{M}} = [\boldsymbol{H}_{1,R,\mathcal{M}}, \boldsymbol{H}_{2,R,\mathcal{M}}, ..., \boldsymbol{H}_{K,R,\mathcal{M}}]$ denotes the channel matrix between each user and each IRS. $\boldsymbol{\Theta}_m = \mathrm{diag}(\theta_{m,1}, \theta_{m,2}, ..., \theta_{m,N_\mathrm{I}})$ represents the passive beamformer of IRS m (we assume that the IRS can adjust only the phase shift, i.e., $|\theta_{m,n}| = 1$), $\boldsymbol{\Theta} = \mathrm{diag}(\{\boldsymbol{\Theta}_m\}_{m\in\mathcal{M}})$, $\boldsymbol{F}_{\mathcal{K}} = \mathrm{diag}(\{\boldsymbol{F}_k\}_{k\in\mathcal{K}})$, and $\boldsymbol{s}_{\mathcal{K}} = [\boldsymbol{s}_1^{\mathrm{T}}, \boldsymbol{s}_2^{\mathrm{T}}, ..., \boldsymbol{s}_K^{\mathrm{T}}]^{\mathrm{T}}$. Finally, $\boldsymbol{n}_l \sim \mathcal{CN}(\boldsymbol{0}, \sigma^2\boldsymbol{I})$ is the additive white Gaussian noise. In the system, each IRS is deployed near an RRH, and the distance between two arbitrary IRSs is quite large. Therefore, the double reflection among the IRSs is ignored due to the large path-loss.

RRH l compresses its received signals and then transmits the quantization bits to the BBU pool through a wired fronthaul link with limited capacity. By adopting the Gaussian test channel model, the compressed signal recovered by the BBU pool can be expressed as follows (Park et al., 2014):

$$\hat{\boldsymbol{y}}_l = \boldsymbol{y}_l + \boldsymbol{q}_l, \tag{3}$$

where $\boldsymbol{q}_l \sim \mathcal{CN}(\boldsymbol{0}, \boldsymbol{\Omega}_l)$ represents the quantization noise for RRH l and $\boldsymbol{\Omega}_l$ denotes its covariance matrix which is determined by the corresponding quantization codebook.

3 Joint design of beamforming and fronthaul compression under P2P compression

In this section we investigate the joint design of user transmit beamformers, IRS passive beamformers, and fronthaul compression when each RRH conducts P2P compression, aiming to maximize the system uplink sum rate.

3.1 Problem formulation

From Eqs. (1) and (3), the achievable uplink sum rate of the considered C-RAN is given by

$$\begin{aligned}R_{\mathrm{sum}} =& I(\boldsymbol{s}_{\mathcal{K}}; \hat{\boldsymbol{y}}_{\mathcal{L}}) \\ =& \log_2\left|\boldsymbol{V}_{\mathcal{L}}\boldsymbol{F}_{\mathcal{K}}\boldsymbol{F}_{\mathcal{K}}\boldsymbol{V}_{\mathcal{L}}^{\mathrm{H}} + \sigma^2\boldsymbol{I} + \boldsymbol{\Omega}_{\mathcal{L}}\right| \\ &- \log_2\left|\sigma^2\boldsymbol{I} + \boldsymbol{\Omega}_{\mathcal{L}}\right|,\end{aligned} \tag{4}$$

where $I(\cdot;\cdot)$ represents the mutual information, $\hat{\boldsymbol{y}}_{\mathcal{L}} = [\hat{\boldsymbol{y}}_1^{\mathrm{T}}, \hat{\boldsymbol{y}}_2^{\mathrm{T}}, ..., \hat{\boldsymbol{y}}_L^{\mathrm{T}}]^{\mathrm{T}}$, $\boldsymbol{V}_{\mathcal{L}} = \boldsymbol{H}_{\mathcal{L}} + \boldsymbol{G}_{\mathcal{L}}\boldsymbol{\Theta}\boldsymbol{H}_{\mathcal{K},R,\mathcal{M}}$, $\boldsymbol{H}_{\mathcal{L}} = [\boldsymbol{H}_{\mathcal{K},1}^{\mathrm{T}}, \boldsymbol{H}_{\mathcal{K},2}^{\mathrm{T}}, ..., \boldsymbol{H}_{\mathcal{K},L}^{\mathrm{T}}]^{\mathrm{T}}$ denotes the direct link channel matrix between all users and all RRHs, $\boldsymbol{G}_{\mathcal{L}} = [\boldsymbol{G}_{1,\mathcal{M}}^{\mathrm{T}}, \boldsymbol{G}_{2,\mathcal{M}}^{\mathrm{T}}, ..., \boldsymbol{G}_{L,\mathcal{M}}^{\mathrm{T}}]^{\mathrm{T}}$ denotes the channel matrix between all IRSs and all RRHs, and $\boldsymbol{\Omega}_{\mathcal{L}} = \mathrm{diag}(\{\boldsymbol{\Omega}_l\}_{l\in\mathcal{L}})$.

The compression rate at each RRH should not exceed the fronthaul link capacity. Under P2P compression, the corresponding fronthaul constraints are given by the following expression (Park et al., 2014):

$$I(\boldsymbol{y}_l; \hat{\boldsymbol{y}}_l) \le C_l,\ \forall l \in \mathcal{L}, \tag{5}$$

where C_l represents the fronthaul capacity from RRH l to the BBU pool. According to Eqs. (2) and (3), the random variables in the mutual information term on the left jointly follow the Gaussian distribution. Let $\boldsymbol{V}_l = \boldsymbol{H}_{\mathcal{K},l} + \boldsymbol{G}_{l,\mathcal{M}}\boldsymbol{\Theta}\boldsymbol{H}_{\mathcal{K},R,\mathcal{M}}$. Constraint (5) can be expressed as

$$\log_2\left|\boldsymbol{V}_l\boldsymbol{F}_{\mathcal{K}}\boldsymbol{F}_{\mathcal{K}}\boldsymbol{V}_l^{\mathrm{H}} + \sigma^2\boldsymbol{I} + \boldsymbol{\Omega}_l\right| - \log_2\left|\boldsymbol{\Omega}_l\right| \le C_l. \tag{6}$$

With the goal of maximizing the uplink sum rate in Eq. (4) under the fronthaul constraint (6) under P2P compression, we jointly optimize the transmit beamformers of users, the passive beamformers, and the quantization noise covariance matrices for fronthaul compression. The problem is formulated as

follows:

$$\max_{\boldsymbol{F}_k,\boldsymbol{\Theta},\boldsymbol{\Omega}_l}\Big(\log_2|\boldsymbol{V}_{\mathcal{L}}\boldsymbol{F}_{\mathcal{K}}\boldsymbol{F}_{\mathcal{K}}^{\mathrm{H}}\boldsymbol{V}_{\mathcal{L}}^{\mathrm{H}}+\sigma^2\boldsymbol{I}+\boldsymbol{\Omega}_{\mathcal{L}}|-\log_2|\sigma^2\boldsymbol{I}+\boldsymbol{\Omega}_{\mathcal{L}}|\Big)$$

$$\text{s.t.}\begin{cases}\log_2|\boldsymbol{V}_l\boldsymbol{F}_{\mathcal{K}}\boldsymbol{F}_{\mathcal{K}}^{\mathrm{H}}\boldsymbol{V}_l^{\mathrm{H}}+\sigma^2\boldsymbol{I}+\boldsymbol{\Omega}_l|-\log_2|\boldsymbol{\Omega}_l|\le C_l,\\ \mathrm{tr}(\boldsymbol{F}_k\boldsymbol{F}_k^{\mathrm{H}})\le P_k,\forall k\in\mathcal{K},\\ \boldsymbol{\Omega}_l\succeq 0,\forall l\in\mathcal{L},\\ |\theta_{m,n}|=1,\forall m,n.\end{cases}\tag{7}$$

It is non-trivial to find the optimal solution to the above problem, due to the fact that the objective function, the fronthaul constraints, and the constraint $|\theta_{m,n}|=1$ are not convex. In the following subsection, we adopt the SCA approach (Scutari et al., 2014) to make the problem tractable.

3.2 SCA approach

First, for the objective in problem (7), we exploit the Arimoto-Blahut algorithm, which is given by the following lemma:

Lemma 1 (Cover and Thomas, 2006) For a channel with input s, output y, and transition probability $p(y|s)$, the mutual information $I(s;y)$ with an arbitrary input probability distribution $p(s)$ is given by the following expression:

$$I(s;y)=\max_{q(s|y)}\mathbb{E}\left[\log_2\left(\frac{q(s|y)}{p(s)}\right)\right],\tag{8}$$

where the expectation takes all possible s and y generated from the probability distribution $p(s)$ and $p(y|s)$, respectively. The optimal $q^{\circ}(s|y)$ is the posterior probability:

$$q^{\circ}(s|y)=\frac{p(s)p(y|s)}{p(y)}\triangleq p(s|y).\tag{9}$$

Note that the sum rate in Eq. (4) is derived from $I(\boldsymbol{s}_{\mathcal{K}};\hat{\boldsymbol{y}}_{\mathcal{L}})$, where the input probability distribution $p(\boldsymbol{s}_{\mathcal{K}})$ is $\mathcal{CN}(\boldsymbol{0},\boldsymbol{I})$ and the channel transition probability $p(\hat{\boldsymbol{y}}_{\mathcal{L}}|\boldsymbol{s}_{\mathcal{K}})$ is from Eqs. (2) and (3). Then, according to Lemma 1, the sum rate (Eq. (4)) can be rewritten as

$$R_{\mathrm{sum}}=\max_{q(\boldsymbol{s}_{\mathcal{K}}|\hat{\boldsymbol{y}}_{\mathcal{L}})}\mathbb{E}\left[\log_2\frac{q(\boldsymbol{s}_{\mathcal{K}}|\hat{\boldsymbol{y}}_{\mathcal{L}})}{p(\boldsymbol{s}_{\mathcal{K}})}\right],\tag{10}$$

where the optimal $q^*(\boldsymbol{s}_{\mathcal{K}}|\hat{\boldsymbol{y}}_{\mathcal{L}})$ for Eq. (10) is the posterior probability $p(\boldsymbol{s}_{\mathcal{K}}|\hat{\boldsymbol{y}}_{\mathcal{L}})$. According to Theorem 10.3 in Sengijpta (1995), $p(\boldsymbol{s}_{\mathcal{K}}|\hat{\boldsymbol{y}}_{\mathcal{L}})$ follows the complex Gaussian distribution $\mathcal{CN}(\boldsymbol{W}^*\hat{\boldsymbol{y}}_{\mathcal{L}},\boldsymbol{\Sigma}^*)$ with

$$\boldsymbol{W}^*=\boldsymbol{F}_{\mathcal{K}}^{\mathrm{H}}\boldsymbol{V}_{\mathcal{L}}^{\mathrm{H}}\big(\boldsymbol{V}_{\mathcal{L}}\boldsymbol{F}_{\mathcal{K}}\boldsymbol{F}_{\mathcal{K}}^{\mathrm{H}}\boldsymbol{V}_{\mathcal{L}}^{\mathrm{H}}+\sigma^2\boldsymbol{I}+\boldsymbol{\Omega}_{\mathcal{L}}\big)^{-1}\tag{11}$$

and

$$\boldsymbol{\Sigma}^*=\boldsymbol{I}-\boldsymbol{W}^*\boldsymbol{V}_{\mathcal{L}}\boldsymbol{F}_{\mathcal{K}},\tag{12}$$

and the sum rate can be expressed as follows:

$$R_{\mathrm{sum}}=\max_{\boldsymbol{W},\boldsymbol{\Sigma}}\mathbb{E}\left[\log_2\left(\frac{\mathcal{CN}(\boldsymbol{W}\hat{\boldsymbol{y}}_{\mathcal{L}},\boldsymbol{\Sigma})}{\mathcal{CN}(\boldsymbol{0},\boldsymbol{I})}\right)\right].\tag{13}$$

Using the Arimoto-Blahut algorithm, the formula of the achievable sum rate is transformed into an expectation term, with which this non-convex objective function can be transformed into a convex form, as will be discussed later. Then we tackle constraint (6) in problem (7). First, we state the following lemma:

Lemma 2 (Zhou YH and Yu, 2016) For positive definite Hermitian matrices $\boldsymbol{\Gamma},\boldsymbol{E}\in\mathbb{C}^{L\times L}$, we have

$$\log_2|\boldsymbol{\Gamma}|\le\log_2|\boldsymbol{E}|+\mathrm{tr}(\boldsymbol{E}^{-1}\boldsymbol{\Gamma})-L,\tag{14}$$

with equality if and only if $\boldsymbol{\Gamma}=\boldsymbol{E}$.

Then, we rewrite constraint (6) as follows:

$$\log_2|\boldsymbol{\Gamma}_l|-\log_2|\boldsymbol{\Omega}_l|\le C_l,\tag{15}$$

where $\boldsymbol{\Gamma}_l=\boldsymbol{V}_l\boldsymbol{F}_{\mathcal{K}}\boldsymbol{F}_{\mathcal{K}}^{\mathrm{H}}\boldsymbol{V}_l^{\mathrm{H}}+\sigma^2\boldsymbol{I}+\boldsymbol{\Omega}_l$. According to Lemma 2, the first term on the left-hand side (LHS) is upper-bounded by

$$\log_2|\boldsymbol{\Gamma}_l|\le\log_2|\boldsymbol{E}_l|+\mathrm{tr}(\boldsymbol{E}_l^{-1}\boldsymbol{\Gamma}_l)-N_{\mathrm{R}}\tag{16}$$

for $\boldsymbol{E}_l\succeq 0$. The equality is achieved by

$$\boldsymbol{E}_l^*=\boldsymbol{\Gamma}_l.\tag{17}$$

With this, we approximate constraint (6) by the following constraint:

$$\log_2|\boldsymbol{E}_l|+\mathrm{tr}(\boldsymbol{E}_l^{-1}\boldsymbol{\Gamma}_l)-N_{\mathrm{R}}-\log_2|\boldsymbol{\Omega}_l|\le C_l.\tag{18}$$

With Eq. (13) and inequality (18), we reformulate the original problem (7) as follows:

$$\max_{\boldsymbol{E}_l,\boldsymbol{W},\boldsymbol{\Sigma},\boldsymbol{F}_k,\boldsymbol{\Theta},\boldsymbol{\Omega}_l}\mathbb{E}\left[\log_2\left(\frac{\mathcal{CN}(\boldsymbol{W}\hat{\boldsymbol{y}}_{\mathcal{L}},\boldsymbol{\Sigma})}{\mathcal{CN}(\boldsymbol{0},\boldsymbol{I})}\right)\right]$$

$$\text{s.t.}\begin{cases}\log_2|\boldsymbol{E}_l|+\mathrm{tr}(\boldsymbol{E}_l^{-1}\boldsymbol{\Gamma}_l)-N_{\mathrm{R}}-\log_2|\boldsymbol{\Omega}_l|\le C_l,\\ \mathrm{tr}(\boldsymbol{F}_k\boldsymbol{F}_k^{\mathrm{H}})\le P_k,\forall k\in\mathcal{K},\\ \boldsymbol{\Omega}_l\succeq 0,\forall l\in\mathcal{L},\\ |\theta_{m,n}|=1,\forall m,n.\end{cases}\tag{19}$$

Remark 1 According to inequality (16), any feasible solution to problem (19) satisfying constraint (18) also satisfies constraint (6) for problem (7). Therefore, it is also feasible for the original problem.

With the above problem reformulation, we can tackle the original problem (7) using SCA as follows: In each iteration, we first update the auxiliary variables $\boldsymbol{E}_l$, $\boldsymbol{W}$, and $\boldsymbol{\Sigma}$, under fixed $\boldsymbol{F}_k$, $\boldsymbol{\Theta}$, and $\boldsymbol{\Omega}_l$. Obviously, the optimal $\boldsymbol{W}$ and $\boldsymbol{\Sigma}$ are given by Eqs. (11) and (12), respectively. $\boldsymbol{E}_l$ is updated according to Eq. (17). Then, we optimize $\boldsymbol{F}_k$, $\boldsymbol{\Theta}$, and $\boldsymbol{\Omega}_l$ by solving problem (19). The convergence is discussed in Section 4.

3.3 Alternative optimization

In this subsection, we solve problem (19) by an alternative approach. The expectation term in the objective can be evaluated as follows:

$$\begin{aligned}
&-\mathbb{E}\left[\log_2\left(\frac{\mathcal{CN}(\boldsymbol{W}\hat{\boldsymbol{y}}_{\mathcal{L}},\boldsymbol{\Sigma})}{\mathcal{CN}(\boldsymbol{0},\boldsymbol{I})}\right)\right]\\
=&\mathbb{E}[(\boldsymbol{s}_{\mathcal{K}}-\boldsymbol{W}\hat{\boldsymbol{y}}_{\mathcal{L}})^{\mathrm{H}}\boldsymbol{\Sigma}^{-1}(\boldsymbol{s}_{\mathcal{K}}-\boldsymbol{W}\hat{\boldsymbol{y}}_{\mathcal{L}})]\\
&-KN_{\mathrm{U}}+\log_2|\boldsymbol{\Sigma}|\\
=&\mathrm{tr}\left(\boldsymbol{W}^{\mathrm{H}}\boldsymbol{\Sigma}^{-1}\boldsymbol{W}(\boldsymbol{V}_{\mathcal{L}}\boldsymbol{F}_{\mathcal{K}}\boldsymbol{F}_{\mathcal{K}}^{\mathrm{H}}\boldsymbol{V}_{\mathcal{L}}^{\mathrm{H}}+\sigma^2\boldsymbol{I}+\boldsymbol{\Omega}_{\mathcal{L}})\right)\\
&-2\mathrm{Re}\left\{\mathrm{tr}\left(\boldsymbol{F}_{\mathcal{K}}^{\mathrm{H}}\boldsymbol{V}_{\mathcal{L}}^{\mathrm{H}}\boldsymbol{W}^{\mathrm{H}}\boldsymbol{\Sigma}^{-1}\right)\right\}\\
&+\mathrm{tr}(\boldsymbol{\Sigma}^{-1})-KN_{\mathrm{U}}+\log_2|\boldsymbol{\Sigma}|.
\end{aligned}\tag{20}$$

We optimize beamformer $\boldsymbol{F}_k$ under fixed $\boldsymbol{\Theta}$ and $\boldsymbol{\Omega}_l$. Then problem (19) becomes the following subproblem:

$$\begin{aligned}
&\min_{\boldsymbol{F}_k}\Big(\mathrm{tr}\left(\boldsymbol{W}^{\mathrm{H}}\boldsymbol{\Sigma}^{-1}\boldsymbol{W}\boldsymbol{V}_{\mathcal{L}}\boldsymbol{F}_{\mathcal{K}}\boldsymbol{F}_{\mathcal{K}}^{\mathrm{H}}\boldsymbol{V}_{\mathcal{L}}^{\mathrm{H}}\right)\\
&\quad-2\mathrm{Re}\left\{\mathrm{tr}\left(\boldsymbol{F}_{\mathcal{K}}^{\mathrm{H}}\boldsymbol{V}_{\mathcal{L}}^{\mathrm{H}}\boldsymbol{W}^{\mathrm{H}}\boldsymbol{\Sigma}^{-1}\right)\right\}\Big)\\
\text{s.t.}\ &\begin{cases}\log_2|\boldsymbol{E}_l|+\mathrm{tr}(\boldsymbol{E}_l^{-1}\boldsymbol{\Gamma}_l)-N_{\mathrm{R}}-\log_2|\boldsymbol{\Omega}_l|\le C_l,\\ \mathrm{tr}(\boldsymbol{F}_k\boldsymbol{F}_k^{\mathrm{H}})\le P_k,\forall k\in\mathcal{K}.\end{cases}
\end{aligned}\tag{21}$$

It can be verified that the above problem is convex. Therefore, it can be efficiently solved with some standard optimization tools such as CVX (Grant and Boyd, 2014).

Next we optimize $\boldsymbol{\Theta}$ and $\boldsymbol{\Omega}_l$ under fixed $\boldsymbol{F}_k$. The corresponding subproblem with respect to problem (19) is given by

$$\begin{aligned}
&\min_{\boldsymbol{\Theta},\boldsymbol{\Omega}_l}\Big(\mathrm{tr}\left(\boldsymbol{W}^{\mathrm{H}}\boldsymbol{\Sigma}^{-1}\boldsymbol{W}(\boldsymbol{V}_{\mathcal{L}}\boldsymbol{F}_{\mathcal{K}}\boldsymbol{F}_{\mathcal{K}}^{\mathrm{H}}\boldsymbol{V}_{\mathcal{L}}^{\mathrm{H}}+\sigma^2\boldsymbol{I}+\boldsymbol{\Omega}_{\mathcal{L}})\right)\\
&\quad-2\mathrm{Re}\left\{\mathrm{tr}\left(\boldsymbol{F}_{\mathcal{K}}^{\mathrm{H}}\boldsymbol{V}_{\mathcal{L}}^{\mathrm{H}}\boldsymbol{W}^{\mathrm{H}}\boldsymbol{\Sigma}^{-1}\right)\right\}\Big)\\
\text{s.t.}\ &\begin{cases}\log_2|\boldsymbol{E}_l|+\mathrm{tr}(\boldsymbol{E}_l^{-1}\boldsymbol{\Gamma}_l)-N_{\mathrm{R}}-\log_2|\boldsymbol{\Omega}_l|\le C_l,\\ \boldsymbol{\Omega}_l\succeq 0,\forall l\in\mathcal{L},\\ |\theta_{m,n}|=1,\forall m,n.\end{cases}
\end{aligned}\tag{22}$$

Problem (22) is still non-convex due to the constraint $|\theta_{m,n}|=1$. To tackle it, first, the objective function can be rewritten as follows:

$$\begin{aligned}
&\mathrm{tr}\left(\boldsymbol{W}^{\mathrm{H}}\boldsymbol{\Sigma}^{-1}\boldsymbol{W}(\boldsymbol{V}_{\mathcal{L}}\boldsymbol{F}_{\mathcal{K}}\boldsymbol{F}_{\mathcal{K}}^{\mathrm{H}}\boldsymbol{V}_{\mathcal{L}}^{\mathrm{H}}+\sigma^2\boldsymbol{I}+\boldsymbol{\Omega}_{\mathcal{L}})\right)\\
&\quad-2\mathrm{Re}\left\{\mathrm{tr}\left(\boldsymbol{F}_{\mathcal{K}}^{\mathrm{H}}\boldsymbol{V}_{\mathcal{L}}^{\mathrm{H}}\boldsymbol{W}^{\mathrm{H}}\boldsymbol{\Sigma}^{-1}\right)\right\}\\
=&\mathrm{tr}\left(\boldsymbol{\Theta}^{\mathrm{H}}\boldsymbol{G}_{\mathcal{L}}^{\mathrm{H}}\boldsymbol{W}^{\mathrm{H}}\boldsymbol{\Sigma}^{-1}\boldsymbol{W}\boldsymbol{G}_{\mathcal{L}}\boldsymbol{\Theta}\boldsymbol{H}_{\mathcal{K},R,\mathcal{M}}\boldsymbol{F}_{\mathcal{K}}\boldsymbol{F}_{\mathcal{K}}^{\mathrm{H}}\boldsymbol{H}_{\mathcal{K},R,\mathcal{M}}^{\mathrm{H}}\right)\\
&+2\mathrm{Re}\left\{\mathrm{tr}\left(\boldsymbol{\Theta}^{\mathrm{H}}\boldsymbol{G}_{\mathcal{L}}^{\mathrm{H}}\boldsymbol{W}^{\mathrm{H}}\boldsymbol{\Sigma}^{-1}\boldsymbol{W}\boldsymbol{H}_{\mathcal{L}}\boldsymbol{F}_{\mathcal{K}}\boldsymbol{F}_{\mathcal{K}}^{\mathrm{H}}\boldsymbol{H}_{\mathcal{K},R,\mathcal{M}}^{\mathrm{H}}\right)\right\}\\
&-2\mathrm{Re}\left\{\mathrm{tr}\left(\boldsymbol{\Theta}^{\mathrm{H}}\boldsymbol{G}_{\mathcal{L}}^{\mathrm{H}}\boldsymbol{W}^{\mathrm{H}}\boldsymbol{\Sigma}^{-1}\boldsymbol{F}_{\mathcal{K}}^{\mathrm{H}}\boldsymbol{H}_{\mathcal{K},R,\mathcal{M}}^{\boldsymbol{H}}\right)\right\}\\
&+\mathrm{tr}\left(\boldsymbol{W}^{\mathrm{H}}\boldsymbol{\Sigma}^{-1}\boldsymbol{W}\boldsymbol{\Omega}_{\mathcal{L}}\right)\\
&+\mathrm{tr}\left(\boldsymbol{W}^{\mathrm{H}}\boldsymbol{\Sigma}^{-1}\boldsymbol{W}(\boldsymbol{H}_{\mathcal{L}}\boldsymbol{F}_{\mathcal{K}}\boldsymbol{F}_{\mathcal{K}}^{\mathrm{H}}\boldsymbol{H}_{\mathcal{L}}^{\mathrm{H}}+\sigma^2\boldsymbol{I})\right)\\
&-2\mathrm{Re}\left\{\mathrm{tr}\left(\boldsymbol{F}_{\mathcal{K}}^{\mathrm{H}}\boldsymbol{H}_{\mathcal{L}}^{\mathrm{H}}\boldsymbol{W}^{\mathrm{H}}\boldsymbol{\Sigma}^{-1}\right)\right\}\\
\overset{(a)}{=}&\hat{\boldsymbol{\theta}}^{\mathrm{H}}(\boldsymbol{A}\odot\boldsymbol{B}^{\mathrm{T}})\hat{\boldsymbol{\theta}}+2\mathrm{Re}\left\{\mathrm{tr}\left(\hat{\boldsymbol{\theta}}^{\mathrm{H}}\boldsymbol{z}_1\right)\right\}+J_1\\
\overset{(b)}{=}&\mathrm{tr}\left(\boldsymbol{\Psi}\bar{\boldsymbol{\Theta}}\right)+\mathrm{tr}\left(\boldsymbol{W}^{\mathrm{H}}\boldsymbol{\Sigma}^{-1}\boldsymbol{W}\boldsymbol{\Omega}_{\mathcal{L}}\right)+J_1,
\end{aligned}\tag{23}$$

where in (a), we have the following notations:

$$\begin{cases}
\hat{\boldsymbol{\theta}}=\mathrm{diag}(\boldsymbol{\Theta}),\\
\boldsymbol{A}=\boldsymbol{G}_{\mathcal{L}}^{\mathrm{H}}\boldsymbol{W}^{\mathrm{H}}\boldsymbol{\Sigma}^{-1}\boldsymbol{W}\boldsymbol{G}_{\mathcal{L}},\\
\boldsymbol{B}=\boldsymbol{H}_{\mathcal{K},R,\mathcal{M}}\boldsymbol{F}_{\mathcal{K}}\boldsymbol{F}_{\mathcal{K}}^{\mathrm{H}}\boldsymbol{H}_{\mathcal{K},R,\mathcal{M}}^{\mathrm{H}},\\
\boldsymbol{z}_1=\mathrm{diag}\left(\boldsymbol{G}_{\mathcal{L}}^{\mathrm{H}}\boldsymbol{W}^{\mathrm{H}}\boldsymbol{\Sigma}^{-1}\boldsymbol{W}\boldsymbol{H}_{\mathcal{L}}\boldsymbol{F}_{\mathcal{K}}\boldsymbol{F}_{\mathcal{K}}^{\mathrm{H}}\boldsymbol{H}_{\mathcal{K},R,\mathcal{M}}^{\mathrm{H}}\right.\\
\qquad\left.-\boldsymbol{G}_{\mathcal{L}}^{\mathrm{H}}\boldsymbol{W}^{\mathrm{H}}\boldsymbol{\Sigma}^{-1}\boldsymbol{F}_{\mathcal{K}}^{\mathrm{H}}\boldsymbol{H}_{\mathcal{K},R,\mathcal{M}}^{\mathrm{H}}\right),\\
J_1=\mathrm{tr}\left(\boldsymbol{W}^{\mathrm{H}}\boldsymbol{\Sigma}^{-1}\boldsymbol{W}(\boldsymbol{H}_{\mathcal{L}}\boldsymbol{F}_{\mathcal{K}}\boldsymbol{F}_{\mathcal{K}}^{\mathrm{H}}\boldsymbol{H}_{\mathcal{L}}^{\mathrm{H}}+\sigma^2\boldsymbol{I})\right)\\
\qquad-2\mathrm{Re}\left\{\mathrm{tr}(\boldsymbol{F}_{\mathcal{K}}^{\mathrm{H}}\boldsymbol{H}_{\mathcal{L}}^{H}\boldsymbol{W}^{\mathrm{H}}\boldsymbol{\Sigma}^{-1})\right\},
\end{cases}$$

and in (b), we have

$$\begin{cases}
\bar{\boldsymbol{\theta}}=\left[\hat{\boldsymbol{\theta}}^{\mathrm{T}},1\right]^{\mathrm{T}},\\
\bar{\boldsymbol{\Theta}}=\bar{\boldsymbol{\theta}}\bar{\boldsymbol{\theta}}^{\mathrm{H}},\\
\boldsymbol{\Psi}=\begin{pmatrix}\boldsymbol{A}\odot\boldsymbol{B}^{\mathrm{T}} & \boldsymbol{z}_1\\ \boldsymbol{z}_1^{\mathrm{H}} & 0\end{pmatrix}.
\end{cases}$$

Similarly, we can rewrite constraint (18) in problem (19) as follows:

$$\mathrm{tr}(\boldsymbol{\Upsilon}_l\bar{\boldsymbol{\Theta}}) + \mathrm{tr}(\boldsymbol{E}_l^{-1}\boldsymbol{\Omega}_l) - \log_2|\boldsymbol{\Omega}_l| + J_{2,l} \le C_l, \tag{24}$$

where

$$\begin{cases} \boldsymbol{\Upsilon}_l = \begin{pmatrix} \boldsymbol{A}_l \odot \boldsymbol{B}^{\mathrm{T}} & \boldsymbol{z}_{2,l} \\ \boldsymbol{z}_{2,l}^{\mathrm{H}} & 0 \end{pmatrix}, \\ \boldsymbol{A}_l = \boldsymbol{G}_{l,\mathcal{M}}^{\mathrm{H}}\boldsymbol{E}_l^{-1}\boldsymbol{G}_{l,\mathcal{M}}, \\ \boldsymbol{z}_{2,l} = \mathrm{diag}\left(\boldsymbol{G}_{l,\mathcal{M}}^{\mathrm{H}}\boldsymbol{E}_l^{-1}\boldsymbol{H}_{\mathcal{K},l}\boldsymbol{F}_{\mathcal{K}}\boldsymbol{F}_{\mathcal{K}}^{\mathrm{H}}\boldsymbol{H}_{\mathcal{K},R,\mathcal{M}}^{\mathrm{H}}\right), \\ J_{2,l} = \mathrm{tr}\left(\boldsymbol{E}_l^{-1}(\sigma^2\boldsymbol{I} + \boldsymbol{H}_{\mathcal{K},l}\boldsymbol{F}_{\mathcal{K}}\boldsymbol{F}_{\mathcal{K}}^{\mathrm{H}}\boldsymbol{H}_{\mathcal{K},l}^{\mathrm{H}})\right) \\ \qquad + \log_2|\boldsymbol{E}_l| - N_{\mathrm{R}}. \end{cases}$$

The derivation is given in Appendix A.

According to Eq. (23) and inequality (24), the optimization problem (22) becomes

$$\min_{\bar{\boldsymbol{\Theta}},\boldsymbol{\Omega}_l} \left(\mathrm{tr}\left(\boldsymbol{\Psi}\bar{\boldsymbol{\Theta}}\right) + \mathrm{tr}\left(\boldsymbol{W}^{\mathrm{H}}\boldsymbol{\Sigma}^{-1}\boldsymbol{W}\boldsymbol{\Omega}_{\mathcal{L}}\right) + J_1\right)$$

$$\text{s.t.} \begin{cases} \mathrm{tr}\left(\boldsymbol{\Upsilon}_l\bar{\boldsymbol{\Theta}}\right) + \mathrm{tr}\left(\boldsymbol{E}_l^{-1}\boldsymbol{\Omega}_l\right) - \log_2|\boldsymbol{\Omega}_l| + J_{2,l} \le C_l, \\ \mathrm{rank}(\bar{\boldsymbol{\Theta}}) = 1, \\ \bar{\boldsymbol{\Theta}} \succ 0, \\ |\bar{\boldsymbol{\Theta}}_{i,i}| = 1, \forall i, \\ \boldsymbol{\Omega}_l \succeq 0, \forall l \in \mathcal{L}. \end{cases} \tag{25}$$

We apply SDR by relaxing the rank-one constraint on $\bar{\boldsymbol{\Theta}}$, and the resulting problem now becomes convex. Thus, it can be effectively solved by standard convex optimization tools such as CVX. Note that the obtained $\bar{\boldsymbol{\Theta}}$ may not be exactly of rank-one in general. We apply the efficient randomization techniques given in Sidiropoulos et al. (2006) to generate suboptimal candidates and choose the one achieving the minimum objective function.

To this end, we summarize the proposed SCA algorithm for P2P compression (SCA-P2P) (Algorithm 1).

4 Joint design of beamforming and fronthaul compression under Wyner-Ziv coding

In this section we focus on the joint design of beamforming and fronthaul compression under Wyner-Ziv compression. Note that under the P2P compression discussed in Section 3, the BBU pool processes the compressed signals from each RRH individually. Since the received signals at different RRHs are statistically dependent, RRHs can perform more efficient compression (Park et al., 2014) by exploiting this dependency via Wyner-Ziv coding. The BBU pool jointly recovers the compressed signals from all RRHs, whereby the signal dependencies are used as side information. The corresponding fronthaul constraints are given by the following expression (Zhou YH and Yu, 2016):

$$I(\boldsymbol{y}_{\mathcal{S}}; \hat{\boldsymbol{y}}_{\mathcal{S}}|\hat{\boldsymbol{y}}_{\bar{\mathcal{S}}}) \le \sum_{l\in\mathcal{S}} C_l, \ \forall \mathcal{S} \subseteq \mathcal{L}, \tag{26}$$

where $\bar{\mathcal{S}}$ is the complement set of $\mathcal{S}$. Similar to the case of P2P compression, one can evaluate the mutual information term on the left and rewrite constraint (26) as follows:

$$\begin{aligned} &\log_2\left|\boldsymbol{V}_{\mathcal{L}}\boldsymbol{F}_{\mathcal{K}}\boldsymbol{F}_{\mathcal{K}}\boldsymbol{V}_{\mathcal{L}}^{\mathrm{H}} + \sigma^2\boldsymbol{I} + \boldsymbol{\Omega}_{\mathcal{L}}\right| - \log_2|\boldsymbol{\Omega}_{\mathcal{S}}| \\ &- \log_2\left|\boldsymbol{V}_{\bar{\mathcal{S}}}\boldsymbol{F}_{\mathcal{K}}\boldsymbol{F}_{\mathcal{K}}\boldsymbol{V}_{\bar{\mathcal{S}}}^{\mathrm{H}} + \sigma^2\boldsymbol{I} + \boldsymbol{\Omega}_{\bar{\mathcal{S}}}\right| \le C_{\mathcal{S}}, \end{aligned} \tag{27}$$

where

$$\begin{cases} \boldsymbol{V}_{\bar{\mathcal{S}}} = \boldsymbol{H}_{\mathcal{K},\bar{\mathcal{S}}} + \boldsymbol{G}_{\bar{\mathcal{S}},\mathcal{M}}\boldsymbol{\Theta}\boldsymbol{H}_{\mathcal{K},R,\mathcal{M}}, \\ \boldsymbol{\Omega}_{\bar{\mathcal{S}}} = \mathrm{diag}(\{\boldsymbol{\Omega}_l\}_{l\in\bar{\mathcal{S}}}), \\ C_{\mathcal{S}} = \sum\limits_{l\in\mathcal{S}} C_l. \end{cases}$$

With the goal of maximizing the uplink sum rate in Eq. (4) under the fronthaul constraint (27) for Wyner-Ziv coding, the problem is formulated as follows:

$$\max_{\boldsymbol{F}_k,\boldsymbol{\Theta},\boldsymbol{\Omega}_{\mathcal{L}}} \Big(\log_2\left|\boldsymbol{V}_{\mathcal{L}}\boldsymbol{F}_{\mathcal{K}}\boldsymbol{F}_{\mathcal{K}}^{\mathrm{H}}\boldsymbol{V}_{\mathcal{L}}^{\mathrm{H}} + \sigma^2\boldsymbol{I} + \boldsymbol{\Omega}_{\mathcal{L}}\right| - \log_2\left|\sigma^2\boldsymbol{I} + \boldsymbol{\Omega}_{\mathcal{L}}\right|\Big)$$

Algorithm 1 Successive convex approximation for point-to-point compression (SCA-P2P)

1: Initialize $\boldsymbol{F}_k$, $\boldsymbol{\Theta}$, and $\boldsymbol{\Omega}_l$ feasible for problem (7).
2: Update $\boldsymbol{W}$, $\boldsymbol{\Sigma}$, and $\boldsymbol{E}_l$ using Eqs. (11), (12), and (17), respectively.
3: Update $\boldsymbol{F}_k$ by solving the convex problem (21).
4: Solve problem (25). Update $(\boldsymbol{\Theta}, \boldsymbol{\Omega}_l)$ if the objective decreases.
5: Repeat steps 2–4 until convergence.

$$\text{s.t.}\begin{cases}\log_2\left|\boldsymbol{V}_{\mathcal{L}}\boldsymbol{F}_{\mathcal{K}}\boldsymbol{F}_{\mathcal{K}}^{\mathrm{H}}\boldsymbol{V}_{\mathcal{L}}^{\mathrm{H}}+\sigma^2\boldsymbol{I}+\boldsymbol{\Omega}_{\mathcal{L}}\right| \\ \quad -\log_2\left|\boldsymbol{V}_{\bar{\mathcal{S}}}\boldsymbol{F}_{\mathcal{K}}\boldsymbol{F}_{\mathcal{K}}^{\mathrm{H}}\boldsymbol{V}_{\bar{\mathcal{S}}}^{\mathrm{H}}+\sigma^2\boldsymbol{I}+\boldsymbol{\Omega}_{\bar{\mathcal{S}}}\right| \\ \quad -\log_2|\boldsymbol{\Omega}_{\mathcal{S}}|\le C_{\mathcal{S}},\ \forall\mathcal{S}, \\ \mathrm{tr}\left(\boldsymbol{F}_k\boldsymbol{F}_k^{\mathrm{H}}\right)\le P_k,\forall k\in\mathcal{K}, \\ |\theta_{m,n}|=1,\forall m,n, \\ \boldsymbol{\Omega}_l\succeq 0,\forall l\in\mathcal{L}.\end{cases}\tag{28}$$

Again, problem (28) is non-convex and we adopt the SCA to tackle it. Nevertheless, note that the fronthaul constraint (27) for Wyner-Ziv coding cannot be treated in the same way as that for P2P compression, i.e., using solely Lemma 2.

4.1 SCA method

The objective function of problem (28) can be handled similarly as in Section 3. In the following, we focus on the fronthaul constraint (27). First, we rewrite inequality (27) as follows:

$$\begin{aligned}&\log_2|\boldsymbol{\Gamma}_{\mathcal{L}}|-\log|\boldsymbol{\Omega}_{\mathcal{S}}|-\log_2\left|\sigma^2\boldsymbol{I}+\boldsymbol{\Omega}_{\bar{\mathcal{S}}}\right| \\ &-\log_2\left|\frac{\boldsymbol{V}_{\bar{\mathcal{S}}}\boldsymbol{F}_{\mathcal{K}}\boldsymbol{F}_{\mathcal{K}}^{\mathrm{H}}\boldsymbol{V}_{\bar{\mathcal{S}}}^{\mathrm{H}}+\sigma^2\boldsymbol{I}+\boldsymbol{\Omega}_{\bar{\mathcal{S}}}}{\sigma^2\boldsymbol{I}+\boldsymbol{\Omega}_{\bar{\mathcal{S}}}}\right|\le C_{\mathcal{S}},\end{aligned}\tag{29}$$

where $\boldsymbol{\Gamma}_{\mathcal{L}}=\boldsymbol{V}_{\mathcal{L}}\boldsymbol{F}_{\mathcal{K}}\boldsymbol{F}_{\mathcal{K}}^{\mathrm{H}}\boldsymbol{V}_{\mathcal{L}}^{\mathrm{H}}+\sigma^2\boldsymbol{I}+\boldsymbol{\Omega}_{\mathcal{L}}$. The first term on the LHS is similar to inequality (15). Therefore, according to Lemma 2, we have

$$\log_2|\boldsymbol{\Gamma}_{\mathcal{L}}|\le\log_2|\boldsymbol{E}_{\mathcal{L}}|+\mathrm{tr}(\boldsymbol{E}_{\mathcal{L}}^{-1}\boldsymbol{\Gamma}_{\mathcal{L}})-LN_{\mathrm{R}}\tag{30}$$

for $\boldsymbol{E}_{\mathcal{L}}\succeq 0$. The equality is achieved by

$$\boldsymbol{E}_{\mathcal{L}}^{*}=\boldsymbol{\Gamma}_{\mathcal{L}}.\tag{31}$$

The last log-term on the LHS of inequality (29) is equivalent to the mutual information $I(\boldsymbol{s}_{\mathcal{K}};\hat{\boldsymbol{y}}_{\bar{\mathcal{S}}})$, where $\boldsymbol{s}_{\mathcal{K}}$ and $\hat{\boldsymbol{y}}_{\bar{\mathcal{S}}}$ follow joint Gaussian distribution according to Eqs. (1) and (3). By adopting Lemma 1, we have

$$\begin{aligned}&\log_2\left|\frac{\boldsymbol{V}_{\bar{\mathcal{S}}}\boldsymbol{F}_{\mathcal{K}}\boldsymbol{F}_{\mathcal{K}}^{\mathrm{H}}\boldsymbol{V}_{\bar{\mathcal{S}}}^{\mathrm{H}}+\sigma^2\boldsymbol{I}+\boldsymbol{\Omega}_{\bar{\mathcal{S}}}}{\sigma^2\boldsymbol{I}+\boldsymbol{\Omega}_{\bar{\mathcal{S}}}}\right| \\ &\ge\mathbb{E}\left[\log_2\left(\frac{\mathcal{CN}\left(\boldsymbol{W}_{\bar{\mathcal{S}}}\hat{\boldsymbol{y}}_{\bar{\mathcal{S}}},\boldsymbol{\Sigma}_{\bar{\mathcal{S}}}\right)}{\mathcal{CN}(\boldsymbol{0},\boldsymbol{I})}\right)\right],\end{aligned}\tag{32}$$

where equality is achieved by

$$\boldsymbol{W}_{\bar{\mathcal{S}}}^{*}=\boldsymbol{F}_{\mathcal{K}}^{\mathrm{H}}\boldsymbol{V}_{\bar{\mathcal{S}}}^{\mathrm{H}}\left(\boldsymbol{V}_{\bar{\mathcal{S}}}\boldsymbol{F}_{\mathcal{K}}\boldsymbol{F}_{\mathcal{K}}^{\mathrm{H}}\boldsymbol{V}_{\bar{\mathcal{S}}}^{\mathrm{H}}+\sigma^2\boldsymbol{I}+\boldsymbol{\Omega}_{\bar{\mathcal{S}}}\right)^{-1}\tag{33}$$

and

$$\boldsymbol{\Sigma}_{\bar{\mathcal{S}}}^{*}=\boldsymbol{I}-\boldsymbol{W}_{\bar{\mathcal{S}}}^{*}\boldsymbol{V}_{\bar{\mathcal{S}}}\boldsymbol{F}_{\mathcal{K}}.\tag{34}$$

According to inequalities (30) and (32), we can approximate constraint (29) as

$$\begin{aligned}&\log_2|\boldsymbol{E}_{\mathcal{L}}|+\mathrm{tr}(\boldsymbol{E}_{\mathcal{L}}^{-1}\boldsymbol{\Gamma}_{\mathcal{L}})-\mathbb{E}\left[\log_2\left(\frac{\mathcal{CN}(\boldsymbol{W}_{\bar{\mathcal{S}}}\hat{\boldsymbol{y}}_{\bar{\mathcal{S}}},\boldsymbol{\Sigma}_{\bar{\mathcal{S}}})}{\mathcal{CN}(\boldsymbol{0},\boldsymbol{I})}\right)\right] \\ &-\log_2|\boldsymbol{\Omega}_{\mathcal{S}}|-\log_2\left|\sigma^2\boldsymbol{I}+\boldsymbol{\Omega}_{\bar{\mathcal{S}}}\right|-LN_{\mathrm{R}}\le C_{\mathcal{S}}.\end{aligned}\tag{35}$$

Now, with Eq. (20) and inequality (35), we reformulate the original problem (28) as follows:

$$\begin{aligned}\min_{\substack{\boldsymbol{W},\boldsymbol{\Sigma},\boldsymbol{F}_k,\boldsymbol{\Theta},\boldsymbol{\Omega}_{\mathcal{L}}\\ \boldsymbol{E}_{\mathcal{L}},\boldsymbol{W}_{\bar{\mathcal{S}}},\boldsymbol{\Sigma}_{\bar{\mathcal{S}}}}}&\Big(\mathrm{tr}\left(\boldsymbol{W}^{\mathrm{H}}\boldsymbol{\Sigma}^{-1}\boldsymbol{W}(\boldsymbol{V}_{\mathcal{L}}\boldsymbol{F}_{\mathcal{K}}\boldsymbol{F}_{\mathcal{K}}^{\mathrm{H}}\boldsymbol{V}_{\mathcal{L}}^{\mathrm{H}}\right. \\ &\left.+\sigma^2\boldsymbol{I}+\boldsymbol{\Omega}_{\mathcal{L}})\right)-2\mathrm{Re}\left\{\mathrm{tr}\left(\boldsymbol{F}_{\mathcal{K}}^{\mathrm{H}}\boldsymbol{V}_{\mathcal{L}}^{\mathrm{H}}\boldsymbol{W}^{\mathrm{H}}\boldsymbol{\Sigma}^{-1}\right)\right\} \\ &-\mathrm{tr}(\boldsymbol{\Sigma}^{-1})-KN_{\mathrm{U}}+\log_2|\boldsymbol{\Sigma}|\Big) \\ \text{s.t.}&\begin{cases}\text{inequality (35)},\forall\mathcal{S}, \\ |\theta_{m,n}|=1,\forall m,n, \\ \boldsymbol{\Omega}_l\succeq 0,\forall l\in\mathcal{L}.\end{cases}\end{aligned}\tag{36}$$

Similar to the P2P compression case, according to inequalities (30) and (32), any feasible solution to problem (36) is also feasible for the original problem (28). Based on this, we still use SCA to solve problem (28) as follows: In each iteration, we first update the auxiliary variables $\boldsymbol{E}_{\mathcal{L}}$, $\boldsymbol{W}$, $\boldsymbol{\Sigma}$, $\boldsymbol{W}_{\bar{\mathcal{S}}}$, and $\boldsymbol{\Sigma}_{\bar{\mathcal{S}}}$, under fixed $\boldsymbol{F}_k$, $\boldsymbol{\Theta}$, and $\boldsymbol{\Omega}_{\mathcal{L}}$. Obviously, the optimal $\boldsymbol{W}$ and $\boldsymbol{\Sigma}$ are given by Eqs. (11) and (12), respectively. On the other hand, $\boldsymbol{E}_{\mathcal{L}}$, $\boldsymbol{W}_{\bar{\mathcal{S}}}$, and $\boldsymbol{\Sigma}_{\bar{\mathcal{S}}}$ are updated according to Eqs. (31), (33), and (34), respectively. After updating and fixing the auxiliary variables, we optimize $\boldsymbol{F}_k$, $\boldsymbol{\Theta}$, and $\boldsymbol{\Omega}_{\mathcal{L}}$ by solving problem (36).

4.2 Alternative optimization

We solve problem (36) in an alternative manner. First, the expectation term on the LHS of constraint (35) of problem (36) can be evaluated as follows:

$$\begin{aligned}&-\mathbb{E}\left[\log_2\left(\frac{\mathcal{CN}(\boldsymbol{W}_{\bar{\mathcal{S}}}\hat{\boldsymbol{y}}_{\bar{\mathcal{S}}},\boldsymbol{\Sigma}_{\bar{\mathcal{S}}})}{\mathcal{CN}(\boldsymbol{0},\boldsymbol{I})}\right)\right] \\ =&\mathrm{tr}\left(\boldsymbol{W}_{\bar{\mathcal{S}}}^{\mathrm{H}}\boldsymbol{\Sigma}_{\bar{\mathcal{S}}}^{-1}\boldsymbol{W}_{\bar{\mathcal{S}}}(\boldsymbol{V}_{\bar{\mathcal{S}}}\boldsymbol{F}_{\mathcal{K}}\boldsymbol{F}_{\mathcal{K}}^{\mathrm{H}}\boldsymbol{V}_{\bar{\mathcal{S}}}^{\mathrm{H}}+\sigma^2\boldsymbol{I}+\boldsymbol{\Omega}_{\bar{\mathcal{S}}})\right) \\ &-2\mathrm{Re}\left\{\mathrm{tr}\left(\boldsymbol{F}_{\mathcal{K}}^{\mathrm{H}}\boldsymbol{V}_{\bar{\mathcal{S}}}^{\mathrm{H}}\boldsymbol{W}_{\bar{\mathcal{S}}}^{\mathrm{H}}\boldsymbol{\Sigma}_{\bar{\mathcal{S}}}^{-1}\right)\right\} \\ &+\mathrm{tr}\left(\boldsymbol{\Sigma}_{\bar{\mathcal{S}}}^{-1}\right)-KN_{\mathrm{U}}+\log_2|\boldsymbol{\Sigma}_{\bar{\mathcal{S}}}|.\end{aligned}\tag{37}$$

We optimize beamformer $\boldsymbol{F}_k$ under fixed $\boldsymbol{\Theta}$ and $\boldsymbol{\Omega}_{\mathcal{L}}$. Then, problem (36) becomes the following subproblem:

$$\begin{aligned}\min_{\boldsymbol{F}_k}\ &\Big(\mathrm{tr}\left(\boldsymbol{W}^{\mathrm{H}}\boldsymbol{\Sigma}^{-1}\boldsymbol{W}\boldsymbol{V}_{\mathcal{L}}\boldsymbol{F}_{\mathcal{K}}\boldsymbol{F}_{\mathcal{K}}^{\mathrm{H}}\boldsymbol{V}_{\mathcal{L}}^{\mathrm{H}}\right)\\&-2\mathrm{Re}\left\{\mathrm{tr}\left(\boldsymbol{F}_{\mathcal{K}}^{\mathrm{H}}\boldsymbol{V}_{\mathcal{L}}^{\mathrm{H}}\boldsymbol{W}^{\mathrm{H}}\boldsymbol{\Sigma}^{-1}\right)\right\}\Big)\\\text{s.t.}\ &\begin{cases}\mathrm{tr}\left(\boldsymbol{W}_{\bar{\mathcal{S}}}^{\mathrm{H}}\boldsymbol{\Sigma}_{\bar{\mathcal{S}}}^{-1}\boldsymbol{W}_{\bar{\mathcal{S}}}\boldsymbol{V}_{\bar{\mathcal{S}}}\boldsymbol{F}_{\mathcal{K}}\boldsymbol{F}_{\mathcal{K}}^{\mathrm{H}}\boldsymbol{V}_{\bar{\mathcal{S}}}^{\mathrm{H}}\right)\\\quad-2\mathrm{Re}\left\{\mathrm{tr}\left(\boldsymbol{F}_{\mathcal{K}}^{\mathrm{H}}\boldsymbol{V}_{\bar{\mathcal{S}}}^{\mathrm{H}}\boldsymbol{W}_{\bar{\mathcal{S}}}^{\mathrm{H}}\boldsymbol{\Sigma}_{\bar{\mathcal{S}}}^{-1}\right)\right\}\\\quad+\mathrm{tr}\left(\boldsymbol{E}_{\mathcal{L}}^{-1}\boldsymbol{V}_{\mathcal{L}}\boldsymbol{F}_{\mathcal{K}}\boldsymbol{F}_{\mathcal{K}}^{\mathrm{H}}\boldsymbol{V}_{\mathcal{L}}^{\mathrm{H}}\right)+J_3\le C_{\mathcal{S}},\\\mathrm{tr}\left(\boldsymbol{F}_k\boldsymbol{F}_k^{\mathrm{H}}\right)\le P_k,\end{cases}\end{aligned}\tag{38}$$

where

$$\begin{aligned}J_3=&\log_2|\boldsymbol{E}_{\mathcal{L}}|+\mathrm{tr}(\boldsymbol{E}_{\mathcal{L}}^{-1}(\sigma^2\boldsymbol{I}+\boldsymbol{\Omega}_{\mathcal{L}}))-LN_{\mathrm{R}}\\&+\mathrm{tr}(\boldsymbol{W}_{\bar{\mathcal{S}}}^{\mathrm{H}}\boldsymbol{\Sigma}_{\bar{\mathcal{S}}}^{-1}\boldsymbol{W}_{\bar{\mathcal{S}}}(\sigma^2\boldsymbol{I}+\boldsymbol{\Omega}_{\bar{\mathcal{S}}}))\\&+\mathrm{tr}(\boldsymbol{\Sigma}_{\bar{\mathcal{S}}}^{-1})-KN_{\mathrm{U}}+\log_2|\boldsymbol{\Sigma}_{\bar{\mathcal{S}}}|\\&-\log_2|\sigma^2\boldsymbol{I}+\boldsymbol{\Omega}_{\bar{\mathcal{S}}}|-\log_2|\boldsymbol{\Omega}_{\mathcal{S}}|.\end{aligned}$$

Problem (38) is a convex problem, so it can be solved by CVX modeling.

Next, we optimize $\boldsymbol{\Theta}$ and $\boldsymbol{\Omega}_{\mathcal{L}}$ under fixed $\boldsymbol{F}_k$. The subproblem is given by

$$\begin{aligned}\min_{\boldsymbol{\Theta},\boldsymbol{\Omega}_{\mathcal{L}}}\ &\Big(\mathrm{tr}\left(\boldsymbol{W}^{\mathrm{H}}\boldsymbol{\Sigma}^{-1}\boldsymbol{W}(\boldsymbol{V}_{\mathcal{L}}\boldsymbol{F}_{\mathcal{K}}\boldsymbol{F}_{\mathcal{K}}^{\mathrm{H}}\boldsymbol{V}_{\mathcal{L}}^{\mathrm{H}}+\sigma^2\boldsymbol{I}+\boldsymbol{\Omega}_{\mathcal{L}})\right)\\&-2\mathrm{Re}\left\{\mathrm{tr}\left(\boldsymbol{F}_{\mathcal{K}}^{\mathrm{H}}\boldsymbol{V}_{\mathcal{L}}^{\mathrm{H}}\boldsymbol{W}^{\mathrm{H}}\boldsymbol{\Sigma}^{-1}\right)\right\}\Big)\\\text{s.t.}\ &\begin{cases}\text{inequality (35)},\forall\mathcal{S},\\\boldsymbol{\Omega}_l\succeq 0,\forall l\in\mathcal{L},\\|\theta_{m,n}|=1,\forall m,n.\end{cases}\end{aligned}\tag{39}$$

Constraint $|\theta_{m,n}|=1$ is non-convex. To tackle it, first, the objective function is rewritten as Eq. (23). Then, constraint (35) in problem (39) can be rewritten as follows:

$$\begin{aligned}&\mathrm{tr}\left(\boldsymbol{\Upsilon}_{\bar{\mathcal{S}}}\bar{\boldsymbol{\Theta}}\right)+\mathrm{tr}\left(\boldsymbol{E}_{\mathcal{L}}^{-1}\boldsymbol{\Omega}_{\mathcal{L}}\right)+\mathrm{tr}\left(\boldsymbol{W}_{\bar{\mathcal{S}}}^{\mathrm{H}}\boldsymbol{\Sigma}_{\bar{\mathcal{S}}}^{-1}\boldsymbol{W}_{\bar{\mathcal{S}}}\boldsymbol{\Omega}_{\bar{\mathcal{S}}}\right)\\&-\log_2|\sigma^2\boldsymbol{I}+\boldsymbol{\Omega}_{\bar{\mathcal{S}}}|-\log_2|\boldsymbol{\Omega}_{\mathcal{S}}|+J_{3,\bar{\mathcal{S}}}\le C_{\mathcal{S}},\end{aligned}\tag{40}$$

where

$$\boldsymbol{\Upsilon}_{\bar{\mathcal{S}}}=\begin{pmatrix}\boldsymbol{A}_{\bar{\mathcal{S}}}\odot\boldsymbol{B}^{\mathrm{T}} & \boldsymbol{z}_{2,\bar{\mathcal{S}}}\\ \boldsymbol{z}_{2,\bar{\mathcal{S}}}^{\mathrm{H}} & 0\end{pmatrix},$$

$$\boldsymbol{A}_{\bar{\mathcal{S}}}=\boldsymbol{G}_{\mathcal{L}}^{\mathrm{H}}\boldsymbol{E}_{\mathcal{L}}^{-1}\boldsymbol{G}_{\mathcal{L}}+\boldsymbol{G}_{\bar{\mathcal{S}},\mathcal{M}}^{\mathrm{H}}\boldsymbol{W}_{\bar{\mathcal{S}}}^{\mathrm{H}}\boldsymbol{\Sigma}_{\bar{\mathcal{S}}}^{-1}\boldsymbol{W}_{\bar{\mathcal{S}}}\boldsymbol{G}_{\bar{\mathcal{S}},\mathcal{M}},$$

$$\begin{aligned}\boldsymbol{z}_{2,\bar{\mathcal{S}}}=&\mathrm{diag}\Big(\boldsymbol{G}_{\mathcal{L}}^{\mathrm{H}}\boldsymbol{E}_{\mathcal{L}}^{-1}\boldsymbol{H}_{\mathcal{L}}\boldsymbol{F}_{\mathcal{K}}\boldsymbol{F}_{\mathcal{K}}^{\mathrm{H}}\boldsymbol{H}_{\mathcal{K},R,\mathcal{M}}^{\mathrm{H}}\\&-\boldsymbol{G}_{\bar{\mathcal{S}},\mathcal{M}}^{\mathrm{H}}\boldsymbol{W}_{\bar{\mathcal{S}}}^{\mathrm{H}}\boldsymbol{\Sigma}_{\bar{\mathcal{S}}}^{-1}\boldsymbol{F}_{\mathcal{K}}^{\mathrm{H}}\boldsymbol{H}_{\mathcal{K},R,\mathcal{M}}^{\mathrm{H}}\\&+\boldsymbol{G}_{\bar{\mathcal{S}},\mathcal{M}}^{\mathrm{H}}\boldsymbol{W}_{\bar{\mathcal{S}}}^{\mathrm{H}}\boldsymbol{\Sigma}_{\bar{\mathcal{S}}}^{-1}\boldsymbol{W}_{\bar{\mathcal{S}}}\boldsymbol{H}_{\mathcal{K},\bar{\mathcal{S}}}\boldsymbol{F}_{\mathcal{K}}\boldsymbol{F}_{\mathcal{K}}^{\mathrm{H}}\boldsymbol{H}_{\mathcal{K},R,\mathcal{M}}^{\mathrm{H}}\Big),\end{aligned}$$

$$\begin{aligned}J_{3,\bar{\mathcal{S}}}=&\log_2|\boldsymbol{E}_{\mathcal{L}}|+\log_2|\boldsymbol{\Sigma}_{\bar{\mathcal{S}}}|-LN_{\mathrm{R}}+\mathrm{tr}(\boldsymbol{\Sigma}_{\bar{\mathcal{S}}}^{-1})\\&+\mathrm{tr}\left(\boldsymbol{E}_{\mathcal{L}}^{-1}(\sigma^2\boldsymbol{I}+\boldsymbol{H}_{\mathcal{L}}\boldsymbol{F}_{\mathcal{K}}\boldsymbol{F}_{\mathcal{K}}^{\mathrm{H}}\boldsymbol{H}_{\mathcal{L}}^{\mathrm{H}})\right)\\&-2\mathrm{Re}\left\{\mathrm{tr}\left(\boldsymbol{F}_{\mathcal{K}}^{\mathrm{H}}\boldsymbol{H}_{\mathcal{K},\bar{\mathcal{S}}}^{\mathrm{H}}\boldsymbol{W}_{\bar{\mathcal{S}}}^{\mathrm{H}}\boldsymbol{\Sigma}_{\bar{\mathcal{S}}}^{-1}\right)\right\}-KN_{\mathrm{U}}\\&+\mathrm{tr}\left(\boldsymbol{W}_{\bar{\mathcal{S}}}^{\mathrm{H}}\boldsymbol{\Sigma}_{\bar{\mathcal{S}}}^{-1}\boldsymbol{W}_{\bar{\mathcal{S}}}(\sigma^2\boldsymbol{I}+\boldsymbol{H}_{\mathcal{K},\bar{\mathcal{S}}}\boldsymbol{F}_{\mathcal{K}}\boldsymbol{F}_{\mathcal{K}}^{\mathrm{H}}\boldsymbol{H}_{\mathcal{K},\bar{\mathcal{S}}}^{\mathrm{H}})\right).\end{aligned}$$

The detailed derivation can be found in Appendix B.

According to Eq. (23) and inequality (40), the optimization problem (39) becomes

$$\begin{aligned}\min_{\bar{\boldsymbol{\Theta}},\boldsymbol{\Omega}_{\mathcal{L}}}\ &\left(\mathrm{tr}\left(\boldsymbol{\Psi}\bar{\boldsymbol{\Theta}}\right)+\mathrm{tr}\left(\boldsymbol{W}^{\mathrm{H}}\boldsymbol{\Sigma}^{-1}\boldsymbol{W}\boldsymbol{\Omega}_{\mathcal{L}}\right)+J_1\right)\\\text{s.t.}\ &\begin{cases}\text{inequality (40)},\ \forall\mathcal{S},\\\mathrm{rank}(\bar{\boldsymbol{\Theta}})=1,\\\bar{\boldsymbol{\Theta}}\succ 0,\\|\bar{\Theta}_{i,i}|=1,\ \forall i,\\\boldsymbol{\Omega}_l\ \succeq\ 0,\ \forall l\in\mathcal{L}.\end{cases}\end{aligned}\tag{41}$$

Problem (41) has a similar structure to problem (25). We also exploit SDR to solve the problem. We summarize the proposed SCA-based iterative optimization algorithm under Wyner-Ziv coding (SCA-WZ) (Algorithm 2).

Algorithm 2 Successive convex approximation for Wyner-Ziv coding (SCA-WZ)

1: Initialize $\boldsymbol{F}_k$, $\boldsymbol{\Theta}$, and $\boldsymbol{\Omega}_{\mathcal{L}}$ feasible for problem (28).
2: Update $\boldsymbol{W}$, $\boldsymbol{\Sigma}$, $\boldsymbol{E}_{\mathcal{L}}$, $\boldsymbol{W}_{\bar{\mathcal{S}}}$, and $\boldsymbol{\Sigma}_{\bar{\mathcal{S}}}$ using Eqs. (11), (12), (31), (33), and (34), respectively.
3: Update $\boldsymbol{F}_k$ by solving the convex problem (38).
4: Solve problem (41). Update $(\boldsymbol{\Theta},\boldsymbol{\Omega}_{\mathcal{L}})$ if the objective decreases.
5: Repeat steps 2–4 until convergence.

Remark 2 In this study, we consider the joint design of user transmit beamformers, IRS passive beamformers, and fronthaul compression assuming perfect CSI knowledge. With the CSI error, one approach is to add a "safety region" on the feasible region as shown in Najafi et al. (2019). Explicitly, we can multiply a constant b, which is smaller than "1" on the right-hand side of the first constraint in

problems (7) and (28) (i.e., inequalities (6) and (27)). Then, the proposed algorithms can still be used without modification. Another approach is to calculate the expectation of the system's sum rate and fronthaul compression rate over all possible CSI errors (Zhou G et al., 2020). Then, the resulting problem is different from that considered in this study.

4.3 Simplified design under high SQNR

In Zhou YH and Yu (2016), it was shown that for a C-RAN uplink in high SQNR, i.e., in the case of a large fronthaul capacity, the quantization noise covariance matrices at RRHs are nearly optimal when proportional to the background noise covariance matrices, i.e., $\boldsymbol{\Omega}_l^* \approx \beta_l \boldsymbol{I}$ for RRH l, where $\beta_l > 0$ is chosen to satisfy the fronthaul constraint. Although it was proved for P2P compression and Wyner-Ziv coding with sequential decompression, it is straightforward to extend to the case of Wyner-Ziv coding with joint decompression considered in this work. Therefore, we propose an efficient scheme under high SQNR for both Wyner-Ziv coding and P2P compression. Explicitly, we set $\boldsymbol{\Omega}_l = \beta_l \boldsymbol{I}$ and then jointly optimize $\boldsymbol{F}_k$, $\boldsymbol{\Theta}$, and β_l, wherein the non-convex objective function and constraints can be treated in the same way as before. Since we optimize the scalar β_l instead of the whole covariance matrix $\boldsymbol{\Omega}_l$, the computational complexity can be reduced. Moreover, such $\boldsymbol{\Omega}_l$ can be achieved by low complexity per-antenna signal quantization at each RRH in practice.

4.4 Convergence and complexity analysis

In this subsection, we discuss the convergence of the proposed SCA-P2P algorithm and SCA-WZ algorithm, as well as their computational complexities. In the following paragraphs, we take SCA-WZ as an example for detailed discussion, and the computational complexity for SCA-P2P is similar to that for SCA-WZ.

It can be shown that the SCA-WZ algorithm yields a non-decreasing sequence of objective values for problem (19). Therefore, the algorithm is guaranteed to converge. Explicitly, consider the t^{th} iteration. We define $\boldsymbol{W}^{(t)}$, $\boldsymbol{\Sigma}^{(t)}$, $\boldsymbol{E}_{\mathcal{L}}^{(t)}$, $\boldsymbol{W}_{\bar{\mathcal{S}}}^{(t)}$, $\boldsymbol{\Sigma}_{\bar{\mathcal{S}}}^{(t)}$, $\boldsymbol{F}_k^{(t)}$, $\boldsymbol{\Theta}^{(t)}$, and $\boldsymbol{\Omega}_{\mathcal{L}}^{(t)}$ as the solution to problem (36) in the t^{th} iteration. Herein, the value of the objective function in problem (36) is denoted as $\varepsilon\left(\boldsymbol{W}^{(t)}, \boldsymbol{\Sigma}^{(t)}, \boldsymbol{E}_{\mathcal{L}}^{(t)}, \boldsymbol{W}_{\bar{\mathcal{S}}}^{(t)}, \boldsymbol{\Sigma}_{\bar{\mathcal{S}}}^{(t)}, \boldsymbol{F}_k^{(t)}, \boldsymbol{\Theta}^{(t)}, \boldsymbol{\Omega}_{\mathcal{L}}^{(t)}\right)$.

In step 2, updating $\{\boldsymbol{W}^{(t)}, \boldsymbol{\Sigma}^{(t)}\}$ by Eqs. (11) and (12) results in a non-decreasing objective value. On the other hand, updating the auxiliary variable according to Eqs. (31), (33), and (34) does not affect the objective. Hence, we have

$$\begin{aligned}&\varepsilon\left(\boldsymbol{W}^{(t-1)}, \boldsymbol{\Sigma}^{(t-1)}, \boldsymbol{E}_{\mathcal{L}}^{(t-1)}, \boldsymbol{W}_{\bar{\mathcal{S}}}^{(t-1)}, \boldsymbol{\Sigma}_{\bar{\mathcal{S}}}^{(t-1)}, \right.\\ &\quad\left.\boldsymbol{F}_k^{(t-1)}, \boldsymbol{\Theta}^{(t-1)}, \boldsymbol{\Omega}_{\mathcal{L}}^{(t-1)}\right)\\ &\le \varepsilon\left(\boldsymbol{W}^{(t)}, \boldsymbol{\Sigma}^{(t)}, \boldsymbol{E}_{\mathcal{L}}^{(t)}, \boldsymbol{W}_{\bar{\mathcal{S}}}^{(t)}, \boldsymbol{\Sigma}_{\bar{\mathcal{S}}}^{(t)}, \right.\\ &\quad\left.\boldsymbol{F}_k^{(t-1)}, \boldsymbol{\Theta}^{(t-1)}, \boldsymbol{\Omega}_{\mathcal{L}}^{(t-1)}\right).\end{aligned} \tag{42}$$

For step 3, note that according to inequalities (30) and (32), $\{\boldsymbol{F}_k^{(t-1)}\}$ is still feasible for problem (36) with $\{\boldsymbol{W}^{(t)}, \boldsymbol{\Sigma}^{(t)}, \boldsymbol{E}_{\mathcal{L}}^{(t)}, \boldsymbol{W}_{\bar{\mathcal{S}}}^{(t)}, \boldsymbol{\Sigma}_{\bar{\mathcal{S}}}^{(t)}\}$ updated in step 2. Since problem (38) is convex, updating $\{\boldsymbol{F}_k^{(t-1)}\}$ to the optimal solution makes the objective value non-decreasing. Hence, we also have

$$\begin{aligned}&\varepsilon\left(\boldsymbol{W}^{(t)}, \boldsymbol{\Sigma}^{(t)}, \boldsymbol{E}_{\mathcal{L}}^{(t)}, \boldsymbol{W}_{\bar{\mathcal{S}}}^{(t)}, \boldsymbol{\Sigma}_{\bar{\mathcal{S}}}^{(t)}, \boldsymbol{F}_k^{(t-1)}, \boldsymbol{\Theta}^{(t-1)}, \boldsymbol{\Omega}_{\mathcal{L}}^{(t-1)}\right)\\ &\le \varepsilon\left(\boldsymbol{W}^{(t)}, \boldsymbol{\Sigma}^{(t)}, \boldsymbol{E}_{\mathcal{L}}^{(t)}, \boldsymbol{W}_{\bar{\mathcal{S}}}^{(t)}, \boldsymbol{\Sigma}_{\bar{\mathcal{S}}}^{(t)}, \boldsymbol{F}_k^{(t)}, \boldsymbol{\Theta}^{(t-1)}, \boldsymbol{\Omega}_{\mathcal{L}}^{(t-1)}\right).\end{aligned} \tag{43}$$

Finally, in step 4, since SDR is applied, we solely obtain a suboptimal solution to problem (41). Therefore, we check whether the obtained $\{\boldsymbol{\Theta}^{(t)}, \boldsymbol{\Omega}_{\mathcal{L}}^{(t)}\}$ decreases the objective value compared with that obtained by the solution in the last iteration. Therefore, we have

$$\begin{aligned}&\varepsilon\left(\boldsymbol{W}^{(t)}, \boldsymbol{\Sigma}^{(t)}, \boldsymbol{E}_{\mathcal{L}}^{(t)}, \boldsymbol{W}_{\bar{\mathcal{S}}}^{(t)}, \boldsymbol{\Sigma}_{\bar{\mathcal{S}}}^{(t)}, \boldsymbol{F}_k^{(t)}, \boldsymbol{\Theta}^{(t-1)}, \boldsymbol{\Omega}_{\mathcal{L}}^{(t-1)}\right)\\ &\le \varepsilon\left(\boldsymbol{W}^{(t)}, \boldsymbol{\Sigma}^{(t)}, \boldsymbol{E}_{\mathcal{L}}^{(t)}, \boldsymbol{W}_{\bar{\mathcal{S}}}^{(t)}, \boldsymbol{\Sigma}_{\bar{\mathcal{S}}}^{(t)}, \boldsymbol{F}_k^{(t)}, \boldsymbol{\Theta}^{(t)}, \boldsymbol{\Omega}_{\mathcal{L}}^{(t)}\right).\end{aligned} \tag{44}$$

Base on the above, we can obtain

$$\begin{aligned}&\varepsilon\left(\boldsymbol{W}^{(t-1)}, \boldsymbol{\Sigma}^{(t-1)}, \boldsymbol{E}_{\mathcal{L}}^{(t-1)}, \boldsymbol{W}_{\bar{\mathcal{S}}}^{(t-1)}, \boldsymbol{\Sigma}_{\bar{\mathcal{S}}}^{(t-1)}, \right.\\ &\quad\left.\boldsymbol{F}_k^{(t-1)}, \boldsymbol{\Theta}^{(t-1)}, \boldsymbol{\Omega}_{\mathcal{L}}^{(t-1)}\right)\\ &\le \varepsilon\left(\boldsymbol{W}^{(t)}, \boldsymbol{\Sigma}^{(t)}, \boldsymbol{E}_{\mathcal{L}}^{(t)}, \boldsymbol{W}_{\bar{\mathcal{S}}}^{(t)}, \boldsymbol{\Sigma}_{\bar{\mathcal{S}}}^{(t)}, \boldsymbol{F}_k^{(t)}, \boldsymbol{\Theta}^{(t)}, \boldsymbol{\Omega}_{\mathcal{L}}^{(t)}\right).\end{aligned} \tag{45}$$

According to inequality (45), the value of the objective function keeps increasing in each iteration. As for the stop condition of the algorithm, we set a small constant Δ as the threshold of precision. Let the value of the objective function in the t^{th} iteration be $\varepsilon^{(t)}$. Then, the stop condition of the algorithm is $\left|\varepsilon^{(t)} - \varepsilon^{(t-1)}\right| \le \Delta$.

The computational complexity of the SCA-WZ algorithm is dominated by steps 3 and 4, which involve solving problems (38) and (41). In each iteration, by using the interior point method (Potra and Wright, 2000), problem (38) can be efficiently solved by the polynomial in the problem size given by $KN_{\mathrm{U}}d$, and the size of problem (41) is given by $(MN_{\mathrm{I}})^2+LN_{\mathrm{R}}^2$ (Zhou YH and Yu, 2016). The overall complexity of the SCA-WZ algorithm is given as the product of the number of iterations and the above complexity. The complexity of SCA-P2P can be similarly analyzed; it is of the same order as that of SCA-WZ.

5 Numerical results

5.1 Simulation setup

In the simulation, we consider a C-RAN with four users, two IRSs, and two RRHs. The positions of the two RRHs are (−30, 100, 15) m and (30, 100, 15) m, and the two IRSs are located at (−40, 80, 15) m and (40, 80, 15) m. The users are randomly distributed within a circle centered at the origin with a radius of 30 m, and the height is 1 m. For the channels between the users and RRHs, between the users and IRSs, and between the IRSs and RRHs, we apply the Rician fading model with limited numbers of propagation paths (Kim et al., 2021). For example, the uplink channel between user k and RRH l is modeled as

$$\begin{aligned}\boldsymbol{H}_{k,l}=&\sqrt{u_0\left(\frac{d_{\mathrm{U,R}}}{d_0}\right)^{-\alpha_{\mathrm{U,R}}}}\cdot\sqrt{N_{\mathrm{U}}N_{\mathrm{R}}}\\&\cdot\left(\sqrt{\frac{K_{\mathrm{U,R}}}{K_{\mathrm{U,R}}+1}}\eta_{\mathrm{U,R},0}\boldsymbol{a}_{\mathrm{RRH}}(\nu^r_{k,l,0},\xi^r_{k,l,0})\right.\\&\cdot\boldsymbol{a}^{\mathrm{H}}_{\mathrm{user}}(\nu^t_{k,l,0},\xi^t_{k,l,0})\\&+\sqrt{\frac{1}{K_{\mathrm{U,R}}+1}}\frac{1}{\sqrt{G_{\mathrm{U,R}}}}\sum_{g=1}^{G_{\mathrm{U,R}}}\Big(\eta_{\mathrm{U,R},g}\\&\left.\cdot\boldsymbol{a}_{\mathrm{RRH}}(\nu^r_{k,l,g},\xi^r_{k,l,g})\cdot\boldsymbol{a}^{\mathrm{H}}_{\mathrm{user}}(\nu^t_{k,l,g},\xi^t_{k,l,g})\Big)\right),\end{aligned}\tag{46}$$

where u_0 is the path-loss at distance d_0, and $d_{\mathrm{U,R}}$ and $\alpha_{\mathrm{U,R}}$ denote the distance and path-loss exponent between the user and RRH, respectively. The Rician K-factor is denoted by $K_{\mathrm{U,R}}$, and $G_{\mathrm{U,R}}$ is the total number of non-line-of-sight (NLoS) paths. For the g^{th} path, $\eta_{\mathrm{U,R},g}\sim\mathcal{CN}(0,1)$ is the complex path gain. The array response vector at the RRH, i,e., $\boldsymbol{a}_{\mathrm{RRH}}(\cdot)$, is given by

$$\begin{aligned}\boldsymbol{a}_{\mathrm{RRH}}(\nu^r_{k,l,g},\xi^r_{k,l,g})=&\frac{1}{\sqrt{N_{\mathrm{R}}}}\left[1,...,\mathrm{e}^{\mathrm{j}(N_{\mathrm{Rv}}-1)\nu^r_{k,l,g}}\right]^{\mathrm{T}}\\&\otimes\left[1,...,\mathrm{e}^{\mathrm{j}(N_{\mathrm{Rh}}-1)\xi^r_{k,l,g}}\right]^{\mathrm{T}},\end{aligned}\tag{47}$$

where $\nu^r_{k,l,g}=\pi\sin(\vartheta^r_{k,l,g})$ and $\xi^r_{k,l,g}=\pi\sin(\varphi^r_{k,l,g})\cos(\vartheta^r_{k,l,g})$, and $\vartheta^r_{k,l,g}$ and $\varphi^r_{k,l,g}$ are the vertical and horizontal angles of arrival (AoAs), respectively. N_{Rv} and N_{Rh} denote the numbers of vertical and horizontal antennas at the RRH, respectively. The term $\boldsymbol{a}_{\mathrm{user}}(\nu^t_{k,l,g},\xi^t_{k,l,g})$ is similar to Eq. (47), where $\nu^t_{k,l,g}$ and $\xi^t_{k,l,g}$ can be obtained by the vertical and horizontal angles of departure (AoDs) $\vartheta^t_{k,l,g}$ and $\varphi^t_{k,l,g}$, respectively.

In the simulation, we set the path-loss u_0 to −30 dB when the reference distance d_0=1 m. The path-loss exponents $\alpha_{\mathrm{U,R}}$, $\alpha_{\mathrm{U,I}}$, and $\alpha_{\mathrm{I,R}}$ are set to 3.6, 2.2, and 2.2, respectively. For small-scale fading, we set the Rician factors as $K_{\mathrm{U,I}}$=10 dB, $K_{\mathrm{I,R}}$=10 dB, and $K_{\mathrm{U,R}}$=0 dB (we assume that there is no LoS path for the direct links between users and RRHs). The numbers of NLoS paths are set as $G_{\mathrm{U,I}}$=10, $G_{\mathrm{I,R}}$=4, and $G_{\mathrm{U,R}}$=10, where the vertical and horizontal AoAs (AoDs) of each NLoS path are assumed to be uniformly distributed within $[-\pi/4,\pi/4]$ and $[-\pi/2,\pi/2]$, respectively. Each user or RRH is equipped with a uniform linear array, and each IRS is a uniform planar array. The transmit power of each user is set as P_k=10 dBm. Finally, the Gaussian noise variance is set to −87 dBm, and the stop condition threshold is set as $\Delta=10^{-2}$.

5.2 Simulation results

First, we verify the convergence of the proposed algorithms under different numbers of reflection elements per IRS (Fig. 2), wherein "WZ-simp" and "P2P-simp" denote the low-complexity schemes designed for the high SQNR regime where we set $\boldsymbol{\Omega}_l=\beta_l\boldsymbol{I}$. It can be observed that the uplink sum rate gradually increases as the number of iterations rises, and that all the proposed algorithms converge in all cases and have good convergence performance. Comparing the convergence speeds for the schemes with the number of reflection elements as 30 and 70, it can be found that more iterations are required with

a larger number of reflection elements. Moreover, it is shown that the iteration numbers of the simplified algorithms for high SQNR, i.e., "WZ-simp" and "P2P-simp," are smaller than those of "SCA-WZ" and "SCA-P2P," respectively.

Fig. 3 plots the average achieved uplink sum rate of the proposed algorithms versus the number of reflection elements per IRS. For both Wyner-Ziv coding and P2P compression, we also simulate the following cases: (1) "b bits": in practice, the phase of the IRS cannot be continuous; therefore, the IRS phase shift takes 2^b discrete values, i.e., $\theta_{m,n} = \{1, \mathrm{e}^{\mathrm{j}\frac{2\pi}{2^b}}, ..., \mathrm{e}^{\mathrm{j}\frac{(2^b-1)2\pi}{2^b}}\}$. In this case the optimized IRS phase shifts obtained by the SCA-WZ and SCA-P2P algorithms are projected to the nearest discrete values, and $\boldsymbol{\Omega}_l$ is scaled to meet the fronthaul constraints. (2) "Random": IRS phase shifts are uniformly distributed within $[0, 2\pi)$, while only $\boldsymbol{F}_k$ and $\boldsymbol{\Omega}_l$ are optimized. (3) "No IRS": the IRS is removed while $\boldsymbol{F}_k$ and $\boldsymbol{\Omega}_l$ are optimized. In Fig. 3, it can be observed that for both Wyner-Ziv coding and P2P compression, the achieved sum rate increases along with the increase of N_{I}. It shows that deploying IRSs can enhance the system performance, especially with the proposed optimization algorithms, compared with the "no IRS" case. Furthermore, the restriction for the discrete IRS phase shift to 2 bits solely brings limited rate loss. Finally, Wyner-Ziv coding generally outperforms P2P compression, in accordance with the literature.

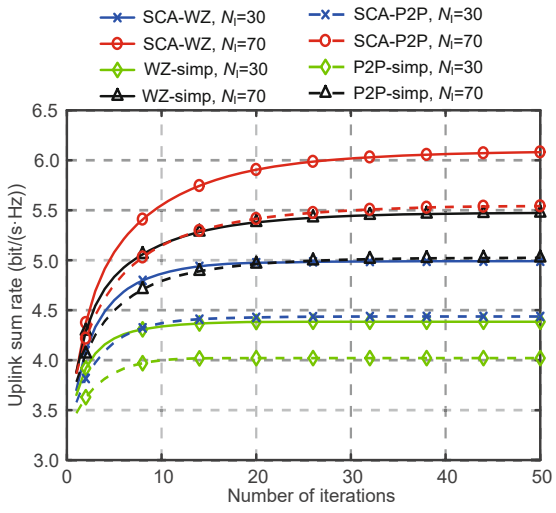

Fig. 2 Average sum rate versus the number of iterations (P_k =10 dBm, C_l =5 bits/(s·Hz), $\forall l$, $N_{\mathrm{R}} = 4$, $N_{\mathrm{U}} = 2$)

Next, we investigate the performance of the proposed algorithms under different numbers of RRH antennas but fixed numbers of user antennas and IRS elements. It can be seen from Fig. 4 that the uplink sum rate increases along with the increase of the number of RRH antennas. This verifies the receiving array gain brought about by the two multi-antenna RRHs. Similar to Fig. 3, the proposed algorithms SCA-WZ and SCA-P2P still outperform all the benchmark schemes under all numbers of RRH antennas.

Fig. 5 plots the average uplink sum rate achieved by the proposed algorithms for Wyner-Ziv coding and P2P compression as well as the low-complexity schemes for high SQNR, wherein the user transmit power is set as P_k = 10 dBm and each IRS has 50

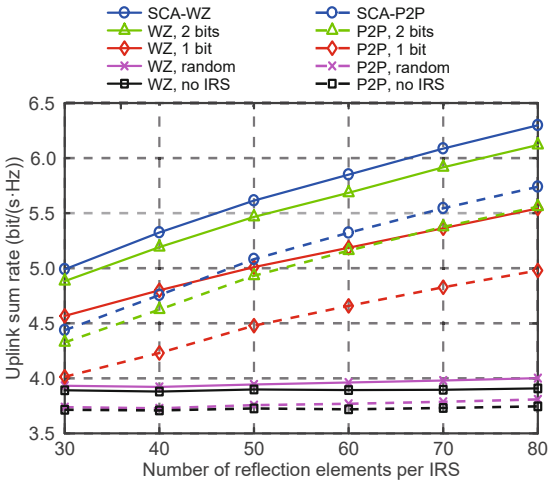

Fig. 3 Average sum rate versus the number of reflection elements per IRS (P_k =10 dBm, C_l = 5 bits/(s·Hz), $\forall l$, $N_{\mathrm{R}} = 4$, $N_{\mathrm{U}} = 2$)

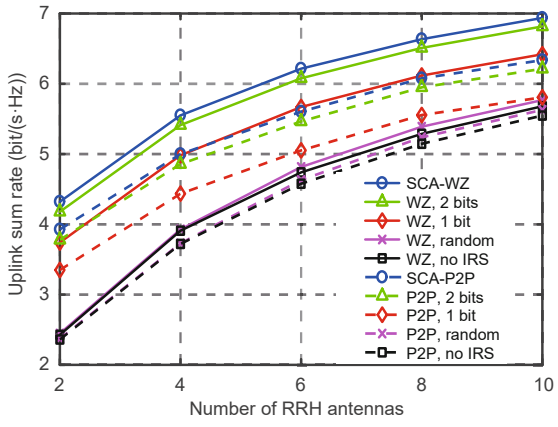

Fig. 4 Average sum rate versus the number of RRH antennas (P_k =10 dBm, N_{I} =50, N_{U} = 2, C_l =5 bits/(s·Hz), $\forall l$)

reflection elements. As the sum fronthaul capacity increases, the rate loss of "WZ-simp" and "P2P-simp" becomes smaller. This validates the premise that setting the quantization covariance matrix proportional to the identity matrix is nearly optimal under high SQNR. It can also be observed that "SCA-WZ" and "WZ-simp" always outperform "SCA-P2P" and "P2P-simp," respectively, as the fronthaul capacity increases.

Finally, we simulate the system's sum rate achieved by the proposed algorithms and the benchmarks under different numbers of IRSs (the number of reflection units for each IRS reflection unit is set to 30). In the simulation, we consider a C-RAN with four users and two RRHs. The positions of the two RRHs are (−30, 100, 15) m and (30, 100, 15) m, and the users are randomly distributed within a circle centered at the origin with a radius of 30 m, and the height is 1 m. The locations of IRSs are: A(−40, 80, 15) m, B(40, 80, 15) m, C(−40, 80, 20) m, and D(40, 80, 20) m.

The simulation results are shown in Table 1. It can be observed that the uplink sum rate increases with the increase of the number of IRSs, and that the proposed algorithms still outperform the corresponding benchmarks. Therefore, the uplink sum rate can be improved by increasing the number of IRSs or the number of reflection elements per IRS. This also verifies that deploying IRSs can enhance the performance of the system.

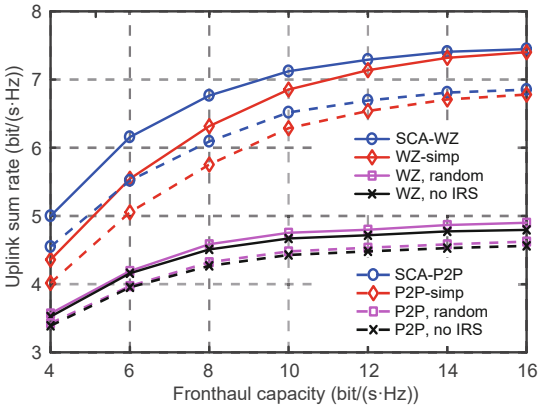

Fig. 5 Average sum rate versus the sum fronthaul capacity (P_k =10 dBm, N_I =50, N_R = 4, N_U = 2)

Table 1 Average sum rate versus the number of IRSs

Algorithm	Average sum rate (bit/(s·Hz))			
	1 IRS	2 IRSs	3 IRSs	4 IRSs
SCA-WZ	4.462	4.949	5.424	5.785
WZ, random	3.836	3.836	3.900	3.934
SCA-P2P	3.966	4.500	4.849	5.180
P2P, random	3.682	3.704	3.751	3.771

The average sum rates are 3.835 and 3.673 bits/(s·Hz) for WZ and P2P, respectively, when there is no IRS. Active IRSs for each case: 1 IRS: A; 2 IRSs: A and B; 3 IRSs: A, B, and C; 4 IRSs: A, B, C, and D. Simulation setting: P_k=10 dBm, C_l=5 bits/(s·Hz), N_R=4, N_U=2, N_I=30

6 Conclusions

In this paper, we have studied a joint design of user transmit beamforming, IRS passive beamforming, and fronthual compression for multi-IRS-aided C-RAN uplink under P2P compression and Wyner-Ziv coding compression, aiming at maximizing the uplink sum rate. We have used the Arimoto-Blahut algorithm and an SDR to handle the non-convex objective function and constraints. Then a successive approximation and optimization approach has been proposed. Based on the approach two iterative optimization algorithms for P2P and WZ have been given. Numerical results have verified that deploying IRSs can considerably improve the C-RAN uplink sum rate with the proposed optimization algorithms.

As for the network energy consumption for uplink transmission, in this work, we have considered solely the transmit power. In practice, the energy consumed by RRHs, IRSs, and fronthauls for data processing and system operation should also be considered. Therefore, the joint design of beamforming and fronthaul compression to improve the network energy efficiency can be a possible extension of the current work.

Contributors

Yu ZHANG and Xuelu WU designed the research. Xuelu WU processed the data and drafted the paper. Yu ZHANG helped organize the paper. Yu ZHANG, Hong PENG, Caijun ZHONG, and Xiaoming CHEN revised and finalized the paper.

Compliance with ethics guidelines

Yu ZHANG, Xuelu WU, Hong PENG, Caijun ZHONG, and Xiaoming CHEN declare that they have no conflict of interest.

References

Blahut R, 1972. Computation of channel capacity and rate-distortion functions. *IEEE Trans Inform Theory*,

18(4):460-473.
https://doi.org/10.1109/TIT.1972.1054855

Cover TM, Thomas JA, 2006. Elements of Information Theory (2nd Ed.). John Wiley & Sons, Inc., Hoboken, New Jersey, USA.

Cui YS, Yin HF, 2019. An efficient CSI acquisition method for intelligent reflecting surface-assisted mmWave networks.
https://arxiv.org/abs/1912.12076v1

Del Coso A, Simoens S, 2009. Distributed compression for MIMO coordinated networks with a backhaul constraint. *IEEE Trans Wirel Commun*, 8(9):4698-4709.
https://doi.org/10.1109/TWC.2009.081148

Grant MC, Boyd SP, 2014. CVX: Matlab Software for Disciplined Convex Programming. http://cvxr.com/cvx/ [Accessed on May 1, 2021].

Guo HY, Liang YC, Chen J, et al., 2019. Weighted sum-rate maximization for intelligent reflecting surface enhanced wireless networks. IEEE Global Communications Conf, p.1-6. https://doi.org/10.1109/GLOBECOM38437.2019.9013288

Hua M, Wu QQ, Ng DWK, et al., 2021. Intelligent reflecting surface-aided joint processing coordinated multipoint transmission. *IEEE Trans Commun*, 69(3):1650-1665.
https://doi.org/10.1109/TCOMM.2020.3042275

Huang SC, Ye Y, Xiao M, et al., 2021. Decentralized beamforming design for intelligent reflecting surface-enhanced cell-free networks. *IEEE Wirel Commun Lett*, 10(3):673-677.
https://doi.org/10.1109/LWC.2020.3045884

Kim S, Lee H, Cha J, et al., 2021. Practical channel estimation and phase shift design for intelligent reflecting surface empowered MIMO systems.
https://arxiv.org/abs/2104.14161v1

Najafi M, Jamali V, Ng DWK, et al., 2019. C-RAN with hybrid RF/FSO fronthaul links: joint optimization of fronthaul compression and RF time allocation. *IEEE Trans Commun*, 67(12):8678-8695.
https://doi.org/10.1109/TCOMM.2019.2940183

Pan CH, Ren H, Wang KZ, et al., 2020. Intelligent reflecting surface aided MIMO broadcasting for simultaneous wireless information and power transfer. *IEEE J Sel Areas Commun*, 38(8):1719-1734.
https://doi.org/10.1109/JSAC.2020.3000802

Park SH, Simeone O, Sahin O, et al., 2013a. Joint precoding and multivariate backhaul compression for the downlink of cloud radio access networks. *IEEE Trans Signal Process*, 61(22):5646-5658.
https://doi.org/10.1109/TSP.2013.2280111

Park SH, Simeone O, Sahin O, et al., 2013b. Robust and efficient distributed compression for cloud radio access networks. *IEEE Trans Veh Technol*, 62(2):692-703.
https://doi.org/10.1109/TVT.2012.2226945

Park SH, Simeone O, Sahin O, et al., 2014. Fronthaul compression for cloud radio access networks: signal processing advances inspired by network information theory. *IEEE Signal Process Mag*, 31(6):69-79.
https://doi.org/10.1109/MSP.2014.2330031

Park SH, Lee KJ, Song C, et al., 2016. Joint design of fronthaul and access links for C-RAN with wireless fronthauling. *IEEE Signal Process Lett*, 23(11):1657-1661.
https://doi.org/10.1109/LSP.2016.2612192

Park SH, Lee KJ, Song C, et al., 2017a. Compressed cooperative reception for the uplink of C-RAN with wireless fronthaul. Int Symp on Wireless Communication Systems, p.211-215.
https://doi.org/10.1109/ISWCS.2017.8108112

Park SH, Song C, Lee KJ, 2017b. Inter-cluster design of wireless fronthaul and access links for the downlink of C-RAN. *IEEE Wirel Commun Lett*, 6(2):270-273.
https://doi.org/10.1109/LWC.2017.2671431

Peng MG, Sun YH, Wang WB, 2020. Intelligent-concise radio access networks in 6G: architecture, techniques and insight. *J Beijing Univ Posts Telecomm*, 43(3):1-10 (in Chinese).
https://doi.org/10.13190/j.jbupt.2020-079

Pizzinat A, Chanclou P, Saliou F, et al., 2015. Things you should know about fronthaul. *J Lightw Technol*, 33(5):1077-1083.
https://doi.org/10.1109/JLT.2014.2382872

Potra FA, Wright SJ, 2000. Interior-point methods. *J Comput Appl Math*, 124(1-2):281-302.
https://doi.org/10.1016/S0377-0427(00)00433-7

Scutari G, Facchinei F, Lampariello L, et al., 2014. Distributed methods for constrained nonconvex multi-agent optimization—part I: theory.
https://arxiv.org/abs/1410.4754v1

Sengijpta SK, 1995. Fundamentals of statistical signal processing: estimation theory. *Technometrics*, 37(4):465-466. https://doi.org/10.1080/00401706.1995.10484391

Sidiropoulos ND, Davidson TN, Luo ZQ, 2006. Transmit beamforming for physical-layer multicasting. *IEEE Trans Signal Process*, 54(6):2239-2251.
https://doi.org/10.1109/TSP.2006.872578

Wang ZR, Liu L, Cui SG, 2020. Channel estimation for intelligent reflecting surface assisted multiuser communications: framework, algorithms, and analysis. *IEEE Trans Wirel Commun*, 19(10):6607-6620.
https://doi.org/10.1109/TWC.2020.3004330

Weinberger K, Ahmad AA, Sezgin A, et al., 2021. Synergistic benefits in IRS- and RS-enabled C-RAN with energy-efficient clustering. https://arxiv.org/abs/2105.05619

Wu QQ, Zhang R, 2018. Intelligent reflecting surface enhanced wireless network: joint active and passive beamforming design. IEEE Global Communications Conf, p.1-6.
https://doi.org/10.1109/GLOCOM.2018.8647620

Wu QQ, Zhang R, 2020. Towards smart and reconfigurable environment: intelligent reflecting surface aided wireless network. *IEEE Commun Mag*, 58(1):106-112.
https://doi.org/10.1109/MCOM.001.1900107

Yu D, Park SH, Simeone O, et al., 2020. Optimizing over-the-air computation in IRS-aided C-RAN systems. IEEE 21st Int Workshop on Signal Processing Advances in Wireless Communications, p.1-5.
https://doi.org/10.1109/SPAWC48557.2020.9154243

Zeng M, Li XW, Li G, et al., 2021. Sum rate maximization for IRS-assisted uplink NOMA. *IEEE Commun Lett*, 25(1):234-238.
https://doi.org/10.1109/LCOMM.2020.3025978

Zhang P, Peng MG, Cui SG, et al., 2022. Theory and techniques for "intellicise" wireless networks. *Front Inform Technol Electron Eng*, 23(1):1-4.
https://doi.org/10.1631/FITEE.2210000

Zhang Y, Zhong CJ, Zhang ZY, et al., 2020. Sum rate optimization for two way communications with intelligent reflecting surface. *IEEE Commun Lett*, 24(5):1090-1094. https://doi.org/10.1109/LCOMM.2020.2978394

Zhang Y, He XX, Zhong CJ, et al., 2021. Fronthaul compression and beamforming optimization for uplink C-RAN with intelligent reflecting surface-enhanced wireless fronthauling. *IEEE Commun Lett*, 25(6):1979-1983. https://doi.org/10.1109/LCOMM.2021.3062861

Zhang ZJ, Dai LL, 2021. A joint precoding framework for wideband reconfigurable intelligent surface-aided cell-free network. *IEEE Trans Signal Process*, 69:4085-4101. https://doi.org/10.1109/TSP.2021.3088755

Zhou G, Pan CH, Ren H, et al., 2020. A framework of robust transmission design for IRS-aided MISO communications with imperfect cascaded channels. *IEEE Trans Signal Process*, 68:5092-5106. https://doi.org/10.1109/TSP.2020.3019666

Zhou YH, Yu W, 2014. Optimized backhaul compression for uplink cloud radio access network. *IEEE J Sel Areas Commun*, 32(6):1295-1307. https://doi.org/10.1109/JSAC.2014.2328133

Zhou YH, Yu W, 2016. Fronthaul compression and transmit beamforming optimization for multi-antenna uplink C-RAN. *IEEE Trans Signal Process*, 64(16):4138-4151. https://doi.org/10.1109/TSP.2016.2563388

Zhu YX, Zheng G, Wong KK, 2020. Stochastic geometry analysis of large intelligent surface-assisted millimeter wave networks. *IEEE J Sel Areas Commun*, 38(8):1749-1762. https://doi.org/10.1109/JSAC.2020.3000806

Appendix A: Derivation of inequality (24)

In the following, we present the derivation from expressions (18) to (24). First, the left-hand side of inequality (18) can be evaluated as follows:

$$\begin{aligned}
&\log_2|\boldsymbol{E}_l| + \mathrm{tr}\left(\boldsymbol{E}_l^{-1}\left(\boldsymbol{V}_l\boldsymbol{F}_{\mathcal{K}}\boldsymbol{F}_{\mathcal{K}}^{\mathrm{H}}\boldsymbol{V}_l^{\mathrm{H}}+\sigma^2\boldsymbol{I}+\boldsymbol{\Omega}_l\right)\right)\\
&\quad -N_{\mathrm{R}}-\log_2|\boldsymbol{\Omega}_l|\\
&=\mathrm{tr}\left(\boldsymbol{G}_{l,\mathcal{M}}^{\mathrm{H}}\boldsymbol{E}_l^{-1}\boldsymbol{G}_{l,\mathcal{M}}\boldsymbol{\Theta}\boldsymbol{B}\boldsymbol{\Theta}^{\mathrm{H}}\right)\\
&\quad +2\mathrm{Re}\left\{\mathrm{tr}\left(\boldsymbol{G}_{l,\mathcal{M}}^{\mathrm{H}}\boldsymbol{E}_l^{-1}\boldsymbol{H}_{\mathcal{K},l}\boldsymbol{F}_{\mathcal{K}}\boldsymbol{F}_{\mathcal{K}}^{\mathrm{H}}\boldsymbol{H}_{\mathcal{K},R,\mathcal{M}}^{\mathrm{H}}\boldsymbol{\Theta}^{\mathrm{H}}\right)\right\}\\
&\quad +\mathrm{tr}\left(\boldsymbol{E}_l^{-1}\boldsymbol{\Omega}_l\right)-\log_2|\boldsymbol{\Omega}_l|+\log_2|\boldsymbol{E}_l|-N_{\mathrm{R}}\\
&\quad +\mathrm{tr}\left(\boldsymbol{E}_l^{-1}\left(\boldsymbol{H}_{\mathcal{K},l}\boldsymbol{F}_{\mathcal{K}}\boldsymbol{F}_{\mathcal{K}}^{\mathrm{H}}\boldsymbol{H}_{\mathcal{K},l}^{\mathrm{H}}+\sigma^2\boldsymbol{I}\right)\right)\\
&\overset{(a)}{=}\hat{\boldsymbol{\theta}}^{\mathrm{H}}(\boldsymbol{A}_l\odot\boldsymbol{B}^{\mathrm{T}})\hat{\boldsymbol{\theta}}+2\mathrm{Re}\left\{\mathrm{tr}\left(\hat{\boldsymbol{\theta}}^{\mathrm{H}}\boldsymbol{z}_{2,l}\right)\right\}+J_{2,l}\\
&\overset{(b)}{=}\mathrm{tr}\left(\boldsymbol{\Upsilon}_l\bar{\boldsymbol{\Theta}}\right)+\mathrm{tr}\left(\boldsymbol{E}_l^{-1}\boldsymbol{\Omega}_l\right)-\log_2|\boldsymbol{\Omega}_l|+J_{2,l},
\end{aligned}\tag{A1}$$

where in (a), we have the following notations:

$$\begin{aligned}
&\hat{\boldsymbol{\theta}}=\mathrm{diag}(\boldsymbol{\Theta}),\\
&\boldsymbol{B}=\boldsymbol{H}_{\mathcal{K},R,\mathcal{M}}\boldsymbol{F}_{\mathcal{K}}\boldsymbol{F}_{\mathcal{K}}^{\mathrm{H}}\boldsymbol{H}_{\mathcal{K},R,\mathcal{M}}^{H},\\
&\boldsymbol{A}_l=\boldsymbol{G}_{l,\mathcal{M}}^{\mathrm{H}}\boldsymbol{E}_l^{-1}\boldsymbol{G}_{l,\mathcal{M}},\\
&\boldsymbol{z}_{2,l}=\mathrm{diag}(\boldsymbol{G}_{l,\mathcal{M}}^{\mathrm{H}}\boldsymbol{E}_l^{-1}\boldsymbol{H}_{\mathcal{K},l}\boldsymbol{F}_{\mathcal{K}}\boldsymbol{F}_{\mathcal{K}}^{\mathrm{H}}\boldsymbol{H}_{\mathcal{K},R,\mathcal{M}}^{\mathrm{H}}),\\
&J_{2,l}=\mathrm{tr}\left(\boldsymbol{E}_l^{-1}(\sigma^2\boldsymbol{I}+\boldsymbol{H}_{\mathcal{K},l}\boldsymbol{F}_{\mathcal{K}}\boldsymbol{F}_{\mathcal{K}}^{\mathrm{H}}\boldsymbol{H}_{\mathcal{K},l}^{\mathrm{H}})\right)\\
&\qquad +\log_2|\boldsymbol{E}_l|-N_{\mathrm{R}},
\end{aligned}$$

and in (b), we have

$$\begin{aligned}
&\bar{\boldsymbol{\theta}}=\left[\hat{\boldsymbol{\theta}}^{\mathrm{T}},1\right]^{\mathrm{T}},\\
&\bar{\boldsymbol{\Theta}}=\bar{\boldsymbol{\theta}}\bar{\boldsymbol{\theta}}^{\mathrm{H}},\\
&\boldsymbol{\Upsilon}_l=\begin{pmatrix}\boldsymbol{A}_l\odot\boldsymbol{B}^{\mathrm{T}} & \boldsymbol{z}_{2,l}\\ \boldsymbol{z}_{2,l}^{\mathrm{H}} & 0\end{pmatrix}.
\end{aligned}$$

Then, we can obtain inequality (24).

Appendix B: Derivation of inequality (40)

In the following, we present the detailed derivation of inequality (40). First, we rewrite the second term on the left-hand side of inequality (35) as follows:

$$\begin{aligned}
&\mathrm{tr}\left(\boldsymbol{E}_{\mathcal{L}}^{-1}\left(\boldsymbol{V}_{\mathcal{L}}\boldsymbol{F}_{\mathcal{K}}\boldsymbol{F}_{\mathcal{K}}^{\mathrm{H}}\boldsymbol{V}_{\mathcal{L}}^{\mathrm{H}}+\sigma^2\boldsymbol{I}+\boldsymbol{\Omega}_{\mathcal{L}}\right)\right)\\
&=\mathrm{tr}\left(\boldsymbol{\Theta}^{\mathrm{H}}\boldsymbol{G}_{\mathcal{L}}^{\mathrm{H}}\boldsymbol{E}_{\mathcal{L}}^{-1}\boldsymbol{G}_{\mathcal{L}}\boldsymbol{\Theta}\boldsymbol{B}\right)\\
&+2\mathrm{Re}\left\{\mathrm{tr}\left(\boldsymbol{\Theta}^{\mathrm{H}}\boldsymbol{G}_{\mathcal{L}}^{\mathrm{H}}\boldsymbol{E}_{\mathcal{L}}^{-1}\boldsymbol{H}_{\mathcal{L}}\boldsymbol{F}_{\mathcal{K}}\boldsymbol{F}_{\mathcal{K}}^{\mathrm{H}}\boldsymbol{H}_{\mathcal{K},R,\mathcal{M}}^{\mathrm{H}}\right)\right\}\\
&+\mathrm{tr}\left(\boldsymbol{E}_{\mathcal{L}}^{-1}\left(\boldsymbol{H}_{\mathcal{L}}\boldsymbol{F}_{\mathcal{K}}\boldsymbol{F}_{\mathcal{K}}^{\mathrm{H}}\boldsymbol{H}_{\mathcal{L}}^{\mathrm{H}}+\sigma^2\boldsymbol{I}\right)\right)+\mathrm{tr}\left(\boldsymbol{E}_{\mathcal{L}}^{-1}\boldsymbol{\Omega}_{\mathcal{L}}\right).
\end{aligned}\tag{B1}$$

Then the expectation term can be evaluated as follows:

$$\begin{aligned}
&-\mathbb{E}\left[\log_2\left(\frac{\mathcal{CN}(\boldsymbol{W}_{\bar{\mathcal{S}}}\hat{\boldsymbol{y}}_{\bar{\mathcal{S}}},\boldsymbol{\Sigma}_{\bar{\mathcal{S}}})}{\mathcal{CN}(\boldsymbol{0},\boldsymbol{I})}\right)\right]\\
&=\mathrm{tr}\left(\boldsymbol{\Theta}^{\mathrm{H}}\boldsymbol{G}_{\bar{\mathcal{S}},\mathcal{M}}^{\mathrm{H}}\boldsymbol{W}_{\bar{\mathcal{S}}}^{\mathrm{H}}\boldsymbol{\Sigma}_{\bar{\mathcal{S}}}^{-1}\boldsymbol{W}_{\bar{\mathcal{S}}}\boldsymbol{G}_{\bar{\mathcal{S}},\mathcal{M}}\boldsymbol{\Theta}\boldsymbol{B}\right)\\
&\quad +2\mathrm{Re}\left\{\mathrm{tr}\left(\boldsymbol{\Theta}^{\mathrm{H}}(\boldsymbol{z}_{\bar{\mathcal{S}},1}-\boldsymbol{z}_{\bar{\mathcal{S}},2})\right)\right\}\\
&\quad +\mathrm{tr}\left(\boldsymbol{W}_{\bar{\mathcal{S}}}^{\mathrm{H}}\boldsymbol{\Sigma}_{\bar{\mathcal{S}}}^{-1}\boldsymbol{W}_{\bar{\mathcal{S}}}\left(\boldsymbol{H}_{\mathcal{K},\bar{\mathcal{S}}}\boldsymbol{F}_{\mathcal{K}}\boldsymbol{F}_{\mathcal{K}}^{\mathrm{H}}\boldsymbol{H}_{\mathcal{K},\bar{\mathcal{S}}}+\sigma^2\boldsymbol{I}\right)\right)\\
&\quad -2\mathrm{Re}\left\{\mathrm{tr}\left(\boldsymbol{F}_{\mathcal{K}}^{\mathrm{H}}\boldsymbol{H}_{\mathcal{K},\bar{\mathcal{S}}}^{\mathrm{H}}\boldsymbol{W}_{\bar{\mathcal{S}}}^{\mathrm{H}}\boldsymbol{\Sigma}_{\bar{\mathcal{S}}}^{-1}\right)\right\}\\
&\quad +\mathrm{tr}(\boldsymbol{\Sigma}_{\bar{\mathcal{S}}}^{-1})-KN_{\mathrm{U}}+\log_2|\boldsymbol{\Sigma}_{\bar{\mathcal{S}}}|,
\end{aligned}\tag{B2}$$

where $\boldsymbol{z}_{\bar{\mathcal{S}},1}=\boldsymbol{G}_{\bar{\mathcal{S}},\mathcal{M}}^{\mathrm{H}}\boldsymbol{W}_{\bar{\mathcal{S}}}^{\mathrm{H}}\boldsymbol{\Sigma}_{\bar{\mathcal{S}}}^{-1}\boldsymbol{W}_{\bar{\mathcal{S}}}\boldsymbol{H}_{\mathcal{K},\bar{\mathcal{S}}}\boldsymbol{F}_{\mathcal{K}}\boldsymbol{F}_{\mathcal{K}}^{\mathrm{H}}\boldsymbol{H}_{\mathcal{K},R,\mathcal{M}}^{\mathrm{H}}$, $\boldsymbol{z}_{\bar{\mathcal{S}},2}=\boldsymbol{G}_{\bar{\mathcal{S}},\mathcal{M}}^{\mathrm{H}}\boldsymbol{W}_{\bar{\mathcal{S}}}^{\mathrm{H}}\boldsymbol{\Sigma}_{\bar{\mathcal{S}}}^{-1}\boldsymbol{F}_{\mathcal{K}}^{\mathrm{H}}\boldsymbol{H}_{\mathcal{K},R,\mathcal{M}}^{\mathrm{H}}$. Then according

to Eqs. (B1) and (B2), we can rewrite the left-hand side of inequality (35) as follows:

$$\begin{aligned}
&\operatorname{tr}\left(\boldsymbol{\Theta}^{\mathrm{H}}\boldsymbol{A}_{\bar{\mathcal{S}}}\boldsymbol{\Theta}\boldsymbol{B}\right)+2\mathrm{Re}\left\{\operatorname{tr}\left(\boldsymbol{\Theta}^{\mathrm{H}}\left(\boldsymbol{z}_{\bar{\mathcal{S}},1}-\boldsymbol{z}_{\bar{\mathcal{S}},2}\right)\right)\right\}\\
&\quad+2\mathrm{Re}\left\{\operatorname{tr}\left(\boldsymbol{\Theta}^{\mathrm{H}}\left(\boldsymbol{G}_{\mathcal{L}}^{\mathrm{H}}\boldsymbol{E}_{\mathcal{L}}^{-1}\boldsymbol{H}_{\mathcal{L}}\boldsymbol{F}_{\mathcal{K}}\boldsymbol{F}_{\mathcal{K}}^{\mathrm{H}}\boldsymbol{H}_{\mathcal{L}}^{\mathrm{H}}\right)\right)\right\}\\
&\quad+\operatorname{tr}\left(\boldsymbol{E}_{\mathcal{L}}^{-1}\boldsymbol{\Omega}_{\mathcal{L}}\right)+\operatorname{tr}\left(\boldsymbol{W}_{\bar{\mathcal{S}}}^{\mathrm{H}}\boldsymbol{\Sigma}_{\bar{\mathcal{S}}}^{-1}\boldsymbol{W}_{\bar{\mathcal{S}}}\boldsymbol{\Omega}_{\bar{\mathcal{S}}}\right)\\
&\quad-\log_2\left|\boldsymbol{\Omega}_{\mathcal{S}}\right|-\log_2\left|\sigma^2\boldsymbol{I}+\boldsymbol{\Omega}_{\bar{\mathcal{S}}}\right|+J_{3,\bar{\mathcal{S}}}\\
&\overset{(a)}{=}\hat{\boldsymbol{\theta}}^{\mathrm{H}}(\boldsymbol{A}_{\bar{\mathcal{S}}}\odot\boldsymbol{B}^{\mathrm{T}})\hat{\boldsymbol{\theta}}+2\mathrm{Re}\{\operatorname{tr}(\hat{\boldsymbol{\theta}}^{\mathrm{H}}\boldsymbol{z}_{2,\bar{\mathcal{S}}})\}\\
&\quad+\operatorname{tr}\left(\boldsymbol{E}_{\mathcal{L}}^{-1}\boldsymbol{\Omega}_{\mathcal{L}}\right)+\operatorname{tr}\left(\boldsymbol{W}_{\bar{\mathcal{S}}}^{\mathrm{H}}\boldsymbol{\Sigma}_{\bar{\mathcal{S}}}^{-1}\boldsymbol{W}_{\bar{\mathcal{S}}}\boldsymbol{\Omega}_{\bar{\mathcal{S}}}\right)\\
&\quad-\log_2\left|\boldsymbol{\Omega}_{\mathcal{S}}\right|-\log_2\left|\sigma^2\boldsymbol{I}+\boldsymbol{\Omega}_{\bar{\mathcal{S}}}\right|+J_{3,\bar{\mathcal{S}}}\\
&\overset{(b)}{=}\operatorname{tr}\left(\boldsymbol{\Upsilon}_{\bar{\mathcal{S}}}\bar{\boldsymbol{\Theta}}\right)+\operatorname{tr}\left(\boldsymbol{E}_{\mathcal{L}}^{-1}\boldsymbol{\Omega}_{\mathcal{L}}\right)+\operatorname{tr}\left(\boldsymbol{W}_{\bar{\mathcal{S}}}^{\mathrm{H}}\boldsymbol{\Sigma}_{\bar{\mathcal{S}}}^{-1}\boldsymbol{W}_{\bar{\mathcal{S}}}\boldsymbol{\Omega}_{\bar{\mathcal{S}}}\right)\\
&\quad-\log_2\left|\sigma^2\boldsymbol{I}+\boldsymbol{\Omega}_{\bar{\mathcal{S}}}\right|-\log_2\left|\boldsymbol{\Omega}_{\mathcal{S}}\right|+J_{3,\bar{\mathcal{S}}},
\end{aligned}\tag{B3}$$

where

$$\begin{cases}
\boldsymbol{A}_{\bar{\mathcal{S}}}=\boldsymbol{G}_{\mathcal{L}}^{\mathrm{H}}\boldsymbol{E}_{\mathcal{L}}^{-1}\boldsymbol{G}_{\mathcal{L}}+\boldsymbol{G}_{\bar{\mathcal{S}},\mathcal{M}}^{\mathrm{H}}\boldsymbol{W}_{\bar{\mathcal{S}}}^{\mathrm{H}}\boldsymbol{\Sigma}_{\bar{\mathcal{S}}}^{-1}\boldsymbol{W}_{\bar{\mathcal{S}}}\boldsymbol{G}_{\bar{\mathcal{S}},\mathcal{M}},\\
\boldsymbol{z}_{2,\bar{\mathcal{S}}}=\operatorname{diag}\left(\boldsymbol{G}_{\mathcal{L}}^{\mathrm{H}}\boldsymbol{E}_{\mathcal{L}}^{-1}\boldsymbol{H}_{\mathcal{L}}\boldsymbol{F}_{\mathcal{K}}\boldsymbol{F}_{\mathcal{K}}^{\mathrm{H}}\boldsymbol{H}_{\mathcal{K},R,\mathcal{M}}^{\mathrm{H}}\right.\\
\qquad\left.-\boldsymbol{z}_{\bar{\mathcal{S}},2}+\boldsymbol{z}_{\bar{\mathcal{S}},1}\right),\\
J_{3,\bar{\mathcal{S}}}=\log_2\left|\boldsymbol{E}_{\mathcal{L}}\right|+\log_2\left|\boldsymbol{\Sigma}_{\bar{\mathcal{S}}}\right|-LN_{\mathrm{R}}+\operatorname{tr}(\boldsymbol{\Sigma}_{\bar{\mathcal{S}}}^{-1})\\
\quad+\operatorname{tr}(\boldsymbol{E}_{\mathcal{L}}^{-1}(\sigma^2\boldsymbol{I}+\boldsymbol{H}_{\mathcal{L}}\boldsymbol{F}_{\mathcal{K}}\boldsymbol{F}_{\mathcal{K}}^{\mathrm{H}}\boldsymbol{H}_{\mathcal{L}}^{\mathrm{H}}))\\
\quad-2\mathrm{Re}\{\operatorname{tr}(\boldsymbol{F}_{\mathcal{K}}^{\mathrm{H}}\boldsymbol{H}_{\mathcal{K},\bar{\mathcal{S}}}^{\mathrm{H}}\boldsymbol{W}_{\bar{\mathcal{S}}}^{\mathrm{H}}\boldsymbol{\Sigma}_{\bar{\mathcal{S}}}^{-1})\}-KN_{\mathrm{U}}\\
\quad+\operatorname{tr}\left(\boldsymbol{W}_{\bar{\mathcal{S}}}^{\mathrm{H}}\boldsymbol{\Sigma}_{\bar{\mathcal{S}}}^{-1}\boldsymbol{W}_{\bar{\mathcal{S}}}(\sigma^2\boldsymbol{I}+\boldsymbol{H}_{\mathcal{K},\bar{\mathcal{S}}}\boldsymbol{F}_{\mathcal{K}}\boldsymbol{F}_{\mathcal{K}}^{\mathrm{H}}\boldsymbol{H}_{\mathcal{K},\bar{\mathcal{S}}}^{\mathrm{H}})\right),\\
\boldsymbol{\Upsilon}_{\bar{\mathcal{S}}}=\begin{pmatrix}\boldsymbol{A}_{\bar{\mathcal{S}}}\odot\boldsymbol{B}^{\mathrm{T}} & \boldsymbol{z}_{2,\bar{\mathcal{S}}}\\ \boldsymbol{z}_{2,\bar{\mathcal{S}}}^{\mathrm{H}} & 0\end{pmatrix}.
\end{cases}$$

Then, we can obtain inequality (40).